In this report, we investigated additional barrier steps of HIV-1 replication in mouse cells and found that the efficiency of viral genome integration into the host chromosome was low in huCD4/CXCR4 Tg mice. As this result suggested an additional barrier in the early steps of viral infection, we examined nuclear transport of the viral genome and demonstrated that integrase (IN)-dependent nuclear import of the preintegration complex (PIC) is blocked in mouse cells.

MATERIALS AND METHODS

Transgene construction. The huCD4 Tg vector (pCT4) was constructed as follows. The 0.85-kb XhoI-EcoRV fragment containing the muCD4 enhancer/promoter was ligated to a 1.8-kb EcoRV-HindIII fragment containing the huCD4 open reading frame, and then a 1.95-kb HindIII-SpeI fragment containing a rabbit β-globin intron sequence and a simian virus 40 (SV40) polyadenylation [poly(A)] signal was inserted into the HindIII-SpeI site downstream of the huCD4 gene (29) (Fig. 1A). To construct the huCXCR4 Tg vector, an XhoI-NotI fragment containing the entire coding region of huCXCR4 was isolated from pBCMGSNeo/HM89 (61), and the huCXCR4 fragment was blunted by T4 DNA polymerase, followed by insertion into the EcoRV site of pCDGH. pCDGH consisted of the muCD4 enhancer/promoter and a human growth hormone gene with its poly(A) signal but devoid of its initiation codon (pCFG) (80) (Fig. 1A). The XhoI-SpeI fragment from pCT4 and the XhoI-NotI fragment from pCFG were then purified and coinjected into the male pronuclei of fertilized mouse eggs (C3H/HeN) (80). The transgenes were detected by dot blot hybridization using DNA prepared from mouse tails (34). Mice were kept under specific-pathogen-free conditions in an environmentally controlled clean room at the Center for Experimental Medicine, the Institute of Medical Science, the University of Tokyo. All equipment and supplies were sterilized, including the cages, water bottles, wood chips, and food pellets. All experiments were conducted according to the institutional ethical and safety guidelines for animal experiments and safety guidelines for gene manipulation experiments.

Northern blot hybridization. Northern blot analyses were carried out as previously described (80). The EcoRV-SpeI fragment of huCD4 and the XhoI-NotI fragment of huCXCR4 used for transgene construction were used as templates to make probes detecting huCD4 and huCXCR4 mRNA, respectively. The autoradiograms were developed, and the radioactivity of each band was quantified with a BAS 2000 Bio-Image analyzer (Fuji Film, Tokyo, Japan).

Plasmids. The HIV-1 pNL4-3 (X4-tropic, accession no. M19921) vector was obtained from A. Adachi (1). The HIV-1 pNL43lucΔenv vector, in which the *env* gene is defective and the *nef* gene is replaced by the firefly luciferase (*Luc*) gene, the pNL4-3 vector containing a mutation at the IN catalytic site (D116G), and an amphotropic Moloney murine leukemia virus (MuLV) envelope expression vector (pJD-1) were kindly provided by T. Masuda (54, 65, 76). A vesicular stomatitis virus G (VSV-G)-expressing plasmid (pMD-G) was obtained from L. Naldini (5, 62). The pGEM/NL-2-LTR plasmid was kindly provided by Y. Koyanagi (73).

The HIV-1 pNL43lucΔenv vector carrying a IN protein tagged with the SV40 nuclear localization signal (NLS) was constructed by using overlap extension PCR (33). First, two different PCRs were performed using HIV-1 pNL43lucΔenv vector as the template: one with the AflII-sense primer, 5′-CATCTTAAGACA GCAGTACAAATGGCAGTA-3′, and NLS-antisense primer, 5′-GGCCTTTC TCTTCTTTTTTGGATCCTCATCCTGTCTACTTGCC-3′, and the other with the NLS-sense primer, 5′-CCAAAAAAGAAGAGAAAGGCCTAACACATG GAAAAGATTAGT-3′, and PflMI-antisense primer, 5′-CTCTTTTTCCTCCA TTCTATGGAGACTCCCTG-3′. These two PCR amplicons were then combined and used as the template for the third PCR with outer primers AflII-sense and PflMI-antisense. The final PCR product was digested with AflII and PflMI and ligated to the SpeI/AflII and SpeI/PflMI vector fragments of HIV-1 pNL43lucΔenv. The nucleotide sequence of the construct was confirmed by sequencing.

To prepare the expression vector for HIV-1 IN N-terminal fusion to enhanced green fluorescence protein (EGFP) (GFP-IN), the entire coding region of HIV-1 IN was amplified by PCR and inserted into the pEGFP-C2 expression vector (Clontech Laboratories, Palo Alto, CA) at its EcoRI and ApaI sites. The primers used to amplify the HIV IN were GFP-IN-sense, 5′-CCGGAATTCCGGGCC ATAGCGGCCTTTTTAGATGGAATAGAT-3′, and GFP-IN-antisense, 5′-TC CGGGCCCGGATTAATCCTCATCCTGTCTACT-3′. To generate the expression vector for the HIV-1 Vpr N or C terminus fused to EGFP (GFP-Vpr, Vpr-GFP), the entire coding region of HIV-1 Vpr was amplified by PCR and inserted into the pEGFP-C2 or pEGFP-N1 expression vector at the HindIII and ApaI or HindIII and BamHI sites, respectively. The primers used to amplify HIV-1 Vpr were GFP-Vpr-sense, 5′-CCCAAGCTTGGGGGACGCCATGGA ACAAGCCCCAGAA-3′, and GFP-Vpr-antisense, 5′-TCCGGGCCCGGACT AGGATCTACTGGCTCCATT-3′, or Vpr-GFP-sense, 5′-CCCAAGCTTGGG GACATGGAACAAGCCCCAGAA-3′, and Vpr-GFP-antisense, 5′-CGCGGA TCCGCGGAGGATCTACTGGCTCCATT-3′, respectively. The amplified regions and the cloning junctions were confirmed by DNA sequencing.

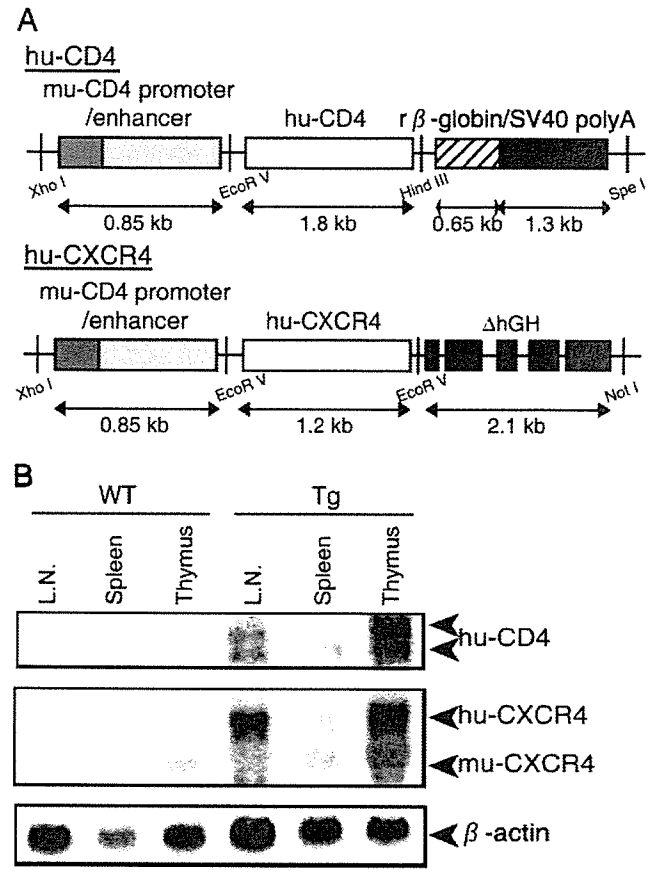

FIG. 1. (A) Transgene constructs. huCD4 or CXCR4 cDNA was placed downstream of the muCD4 enhancer/promoter and ligated to the SV40 poly(A) signal (huCD4) or to a defective human growth hormone gene containing the poly(A) signal (huCXCR4). (B) Transgene expression in lymphatic organs. Northern blot hybridization analysis was performed using 10 μg of total RNA prepared from the thymus, spleen, or lymph nodes of WT or Tg mice. The positions expected for huCD4, huCXCR4, muCXCR4, and β-actin mRNA are indicated on the right.

Cell culture and isolation of human PBMCs and mouse splenocytes and thymocytes. Human fibroblast-like cell lines (293T and HeLa), a mouse embryo fibroblast-like cell line (NIH 3T3) derived from an NIH Swiss mouse (Fv-1^n), and a mouse rectum carcinoma cell line (Colon-26) from a BALB/c mouse (Fv-1^b) were cultured in Dulbecco's modified Eagle's medium (Invitrogen, Tokyo, Japan) supplemented with 10% fetal bovine serum (FBS). The Colon-26 cell line was obtained provided from the Cell Resource Center for Biomedical Research Institute of Development, Aging, and Cancer, Tohoku University, Japan (75). Human T-cell lymphoma cell lines (MT-4 and Jurkat) and mouse T-cell lymphoma cell lines (EL4, YAC-1, and BW5147) were cultured in RPMI 1640 (SIGMA, Tokyo, Japan) containing 10% FBS. Human peripheral blood mononuclear cells (PBMCs) were obtained from peripheral blood. Briefly, buffy coats from the peripheral blood of healthy HIV-seronegative blood donors were separated over a Ficoll-Hypaque gradient (Ficoll-Paque PLUS; GE Healthcare Bio-Sciences, Tokyo, Japan). C3H/HeN mice (Charles River, Tokyo, Japan) were sacrificed at 8 weeks, and the splenocytes and thymocytes were isolated by passage through nylon mesh. Human PBMC suspensions and mouse splenocytes

and thymocytes were stimulated with 1% phytohemagglutinin (SIGMA, Tokyo, Japan). These cells were grown in RPMI 1640 medium containing 4 ng/ml of recombinant human interleukin 2 or mouse interleukin 2 (Peprotech EC Ltd, London, United Kingdom) per ml and 10% FBS. After 1 week, human PBMCs and mouse splenocytes and thymocytes were >96% T cells and >40% activated cells, as judged by fluorescence-activated cell sorter analysis using anti-CD3 or anti-CD69 monoclonal antibodies (BD Biosciences, Tokyo, Japan), respectively (data not shown).

Virus preparation and infection assays. HIV-1 strain NL4-3 was propagated in MT-4 cells, and the supernatants were filtered and stored at −80°C until use. For single-round infection assays, pseudotyped viruses were generated by cotransfection of 293T cells with pNL43lucΔenv vector and an amphotropic Moloney MuLV envelope expression vector (pJD-1) or a VSV-G envelope expression vector (pMD-G) using Lipofectamine PLUS (Invitrogen) (76). The pNL43lucΔenv vector containing a mutation at the IN catalytic site (D116G) was used as a control (54). The culture supernatants of the transfected 293T cells were harvested at 48 h posttransfection, filtered through 0.45-μm filters, and used as the virus preparations. Each virus preparation was treated with DNase I (40 μg/ml; Worthington Biochemical Co., Lakewood, NJ) in the presence of 10 mM $MgCl_2$ at 37°C for 1 h to avoid DNA contamination. An aliquot of each virus preparation was incubated at 65°C for 1 h and used as a heat-inactivated control. To monitor viral gene expression from the pNL43lucΔenv vector carrying a IN protein tagged with the SV40 NLS, luciferase activity in transfected 293T cells was measured on a Lumat LB9507 luminometer (BERTHOLD, Technologies, Bad Wildbad, Germany). At 48 h posttransfection, 293T cells were lysed with 1 ml of luciferase lysis buffer (Promega). One microliter of each cell lysate was subjected to the luciferase assay. Human PBMCs (5×10^6) or HeLa (5×10^5), MT-4 (5×10^6), Jurkat (5×10^6), mouse splenocytes (5×10^6), mouse thymocytes (5×10^6), NIH 3T3 (5×10^5), BW5147 (5×10^6), EL4 (5×10^6), or YAC-1 (5×10^6) cells were infected with an aliquot (2 ml; containing approximately 500 ng [NL4-3], 200 ng [HIV-1/MuLV], or 50 ng [HIV-1/VSV-G] of p24) of DNase-treated virus. The infection proceeded in the presence of Polybrene (SIGMA, Tokyo, Japan) (10 μg/ml) at 37°C. After 6 h, the viruses were removed, and the cells were overlaid with fresh media and incubated at 37°C. For p24 CA analysis, the infected cell supernatants were removed on the indicated days following infection. The levels of HIV-1 p24 antigen were determined by an enzyme immunoassay system (RETRO-TEK; ZeptoMetrix Corp., Buffalo, NY). For luciferase analysis, infected cells were harvested 4 days after infection, and the total cell pellets from each well were washed twice with phosphate-buffered saline (PBS) and lysed in luciferase lysis buffer (Promega). Luciferase activity (measured in a relative light units [RLU]) was measured on a Lumat LB9507 luminometer (BERTHOLD, Technologies, Bad Wildbad, Germany).

Analysis of HIV-1 DNA synthesis and formation of 2-LTR circles. Cells were harvested 24 h after infection. After washing with PBS, nucleic acids were extracted as described previously (81). Briefly, cells were disrupted in urea lysis buffer (4.7 M urea, 1.3%, sodium dodecyl sulfate [SDS], 0.23 M NaCl, 0.67 mM EDTA, and 6.7 mM Tris-HCl [pH 8.0]), phenol-chloroform extracted, and ethanol precipitated. The DNA pellet was resuspended in distilled H_2O, and an aliquot of each sample was analyzed by PCR. For ex vivo infection of primary lymphocytes from huCD4/CXCR4 Tg mice, partial reverse transcripts of the viral DNA were quantified by semiquantitative PCR. The primers used were as follows (37, 45, 81): R-U5, R, 5′-GCCTCAATAAAGCTTGCCTTG-3′ (sense, positions 522 to 542); U5, 5′-CCACTGCTAGAGATTTTCCAC-3′ (antisense, positions 616 to 638); Gag forward, 5′-TGGGGGGACATCAAGCAGCCATG CA-3′ (sense, positions 1360 to 1385); Gag reverse, 5′-CTATGTCACTTCCCC TTGGTTCTCT-3′ (antisense, positions 1474 to 1498). The PCR program was 30 cycles at 95°C for 1 min, 60°C for 1 min, and 72°C for 1 min in the presence of [^{32}P]dCTP. The PCR products were electrophoresed on an 8% polyacrylamide–Tris-borate-EDTA gel. The autoradiograms were developed, and the radioactivity of each band was quantified by a BAS 2000 Bio-Image analyzer. For single-round infections, the DNA was measured by quantitative PCR using an ABI PRISM 7900HT qPCR machine (Applied Biosystems, Tokyo, Japan). The PCR primer pairs were as follows: R-U5 (M667/AA55), R-gag (M667/M661) (76), and the 2-LTR junction's sequence (2-LTR-S/2-LTR-AS) (73). The cycling conditions included a hot start (50°C for 2 min, 95°C for 10 min), followed by 40 cycles of denaturation (95°C for 15 s) and extension (60°C for 1 min). To compensate for varying DNA sample recovery, the data are presented as ratios of HIV-1 DNA to β-actin DNA.

Cassette ligation-mediated PCR and integration analysis. For the detection of the HIV-1 integration form, we designed a cassette ligation-mediated PCR system using an in vitro LA cloning kit (TaKaRa BIO, Shiga, Japan) (35) (see Fig. 3A). Briefly, 5 μg of DNA was digested with EcoRI and ligated to double-stranded DNA cassettes with compatible ends. The cassette-ligated restriction fragments were then subjected to two rounds of PCR using the cassette- and HIV-specific primers C1 (5′-GTACATATTGTCGTTAGAACGCGTAATACG ACTCA-3′) and Gag reverse (described above) for the cassette, *gag*, and its upstream region and C2 (5′-CGTTAGAACGCGTAATACGACTCACTATAG GGAGA-3′) and U5 reverse (described above) for the cassette sequence downstream of C1 and the LTR region. PCR was performed according to the manufacturer's instructions. The amplification conditions were 30 cycles of 1 min at 94°C, 2 min at 54°C, 2 min at 72°C, and a final extension of 1 min at 72°C. The amplified products were resolved on 2% agarose gels and stained with SYBR green (FMC Bioproduct, Rockland, ME).

Fluorescence microscopy. HeLa (4×10^4), NIH 3T3 (3×10^4), and Colon-26 (3×10^4) cells were seeded onto 8-well culture slides (Nalge Nunc International, Rochester, NY) and transfected with the indicated plasmids using Lipofectamine 2000 (Invitrogen). At 24 h posttransfection, the cells were washed once in PBS and fixed with acetone for 5 min. After washing with PBS, the cells were mounted in 90% glycerol–50 mM $NaHCO_3$-Na_2CO_3 and covered by a coverslip. Confocal microscopy was performed with a Nikon Optiphot-2 fluorescence microscope with a Bio-Rad MRC 1024 laser confocal imaging system, and the digital images were prepared using Adobe Photoshop software.

Particle preparation and Western blot analysis. The culture supernatant (5 ml) of HIV-1 producing plasmid-transfected 293T cells was collected at 48 h postinfection. It was centrifuged thorough 20% (wt/vol) sucrose–PBS in an SW55 rotor (Beckman Coulter) at 4°C at 147,000 × *g* for 2 h (56), and the pellet was resuspended in PBS. The viral pellets were hearted at 90°C for 10 min in the presence of sample buffer (62.5 mM Tris-HCl, pH 6.8, 10% glycerol, 2% SDS, 5% 2-mercaptoethanol, 0.005% bromophenol blue). Then viral proteins were electrophoresed on a 12% SDS–polyacrylamide gel containing 0.2% SDS. Following blotting of proteins onto a polyvinylidene difluoride membrane, the membrane was first incubated with an antiserum from an AIDS patient (provided by Y. Inagaki, Tokyo Medical and Dental University, Tokyo, Japan, and Y. Koyanagi, Kyoto University, Kyoto, Japan), followed by horseradish peroxidase-conjugated anti-human immunoglobulin. HIV-1 proteins were visualized using an enhanced chemiluminescence detection system (GE Healthcare Bio-Science, Tokyo, Japan).

Statistical analysis. Data were analyzed using Excel and Student's *t* test. A *P* value of <0.05 was considered statistically significant, and all results are presented as means ± standard errors of the means (SEM).

RESULTS

Lymphocytes from huCD4/CXCR4 Tg mice do not fully support HIV-1 infection. To elucidate the host range barriers of HIV-1 replication in mice, we analyzed the early processes of HIV-1 infection in huCD4/CXCR4 Tg mouse splenocytes. Transgenic mice were generated by introducing both huCD4 and huCXCR4 cDNA along with the muCD4 enhancer/promoter into fertilized C3H mouse eggs (Fig. 1A). As shown in Fig. 1B, the huCD4 and huCXCR4 mRNAs were detected mostly in the thymus but also in the lymph nodes and spleen. Two huCD4 mRNA species were detected due to alternative splicing of the SV40 gene that was ligated to the huCD4 gene (Fig. 1B). fluorescence-activated cell sorter analyses showed that Tg splenocytes and thymocytes both expressed huCD4 and huCXCR4 on their cell surfaces (data not shown).

To examine the susceptibility of these Tg mice to HIV infection, splenocytes and thymocytes were isolated from the mice and infected with T-tropic HIV-1 (NL4-3) or M-tropic HIV-1 (JR-CSF). However, we could not detect any p24 antigen in the culture supernatant of these Tg mouse-derived cells, although significant levels of p24 (up to 80 pg/ml) were produced in human PBMC culture supernatant 12 days after infection.

To determine the process by which the viral replication is blocked, we analyzed the early infection steps by examining the viral genomic structure. Twenty-four hours after HIV-1 infection of the huCD4/CXCR4 Tg splenocytes, cells were har-

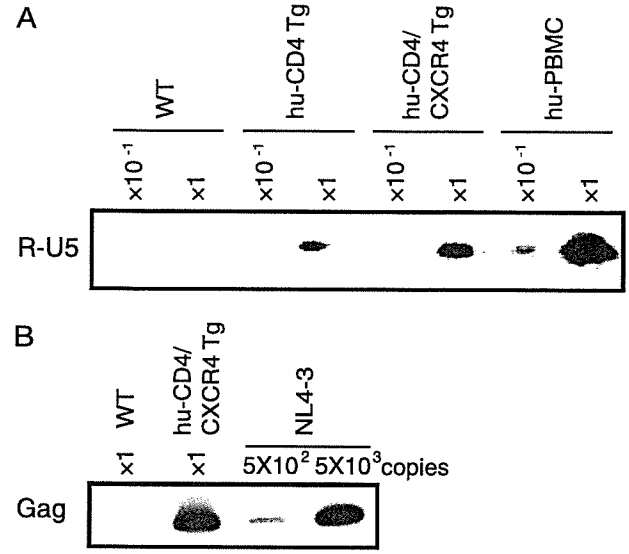

FIG. 2. HIV infection of splenocytes and thymocytes of WT and huCD4/CXCR4 Tg mice. Splenocytes or thymocytes from WT mice, Tg mice, or human PBMCs were isolated and infected with equivalent amounts of DNase-treated NL4-3 virus at 37°C for 6 h. After 6 h, the viruses were removed and the cells were treated with trypsin (500 μg/ml) at 37°C for 10 min and then washed in growth medium. (A and B) Splenocytes were harvested at 24 h postinfection. Total DNA was extracted from the cells and subjected to PCR analysis with a primer pair for R/U5 (A) or R/gag (B). The reaction was carried out using the DNA preparation from 1×10^5 cells (×1) or 1×10^4 cells ($\times 10^{-1}$). In panel B, the lanes marked 5×10^2 and 5×10^3 represent PCR products using 5×10^2 or 5×10^3 copies of the pNL4-3 plasmid as the template.

vested and total DNA was extracted. Early (R-U5) and late-infectious intermediate products (R-gag) were determined using semiquantitative PCR with specific primers. As shown in Fig. 2A and B, both infectious intermediates were detected specifically in the DNA isolated from the splenocytes of huCD4/CXCR4 Tg mice exposed to HIV-1, indicating that viral entry and reverse transcription had proceeded normally in mouse cells provided that human viral receptors were supplied. Similar results were also obtained in huCD4/CCR5 Tg mouse splenocytes infected with HIV-1 JR-CSF (data not shown). In contrast, the early infectious intermediate was not detected in wild-type mouse splenocytes, indicating a block upon viral entry. Taken together, these results suggest that HIV-1 replication in huCD4/CXCR4 Tg splenocytes was blocked later than the reverse transcription step(s).

HIV-1 infection of mouse cells is blocked at steps preceding integration into the host chromosome. We next examined the integration of the HIV-1 genome into the host chromosome. The pNL4-3 vector containing a mutation at the IN catalytic site (D116G) was used as a control (54). DNA from the infected cells was digested with EcoRI, which cut proviral DNA at only one site (nucleotide number 5743 of NL4-3, accession no. M19921). The DNA was then ligated to an EcoRI-specific cassette and subjected to the first round of PCR using primers specific for the cassette and the *gag* region, followed by the second round of PCR using primers for the cassette and the LTR region (Fig. 3A). As a result, the integrated viral DNA was visualized as smearing bands greater than 638 bp, which is

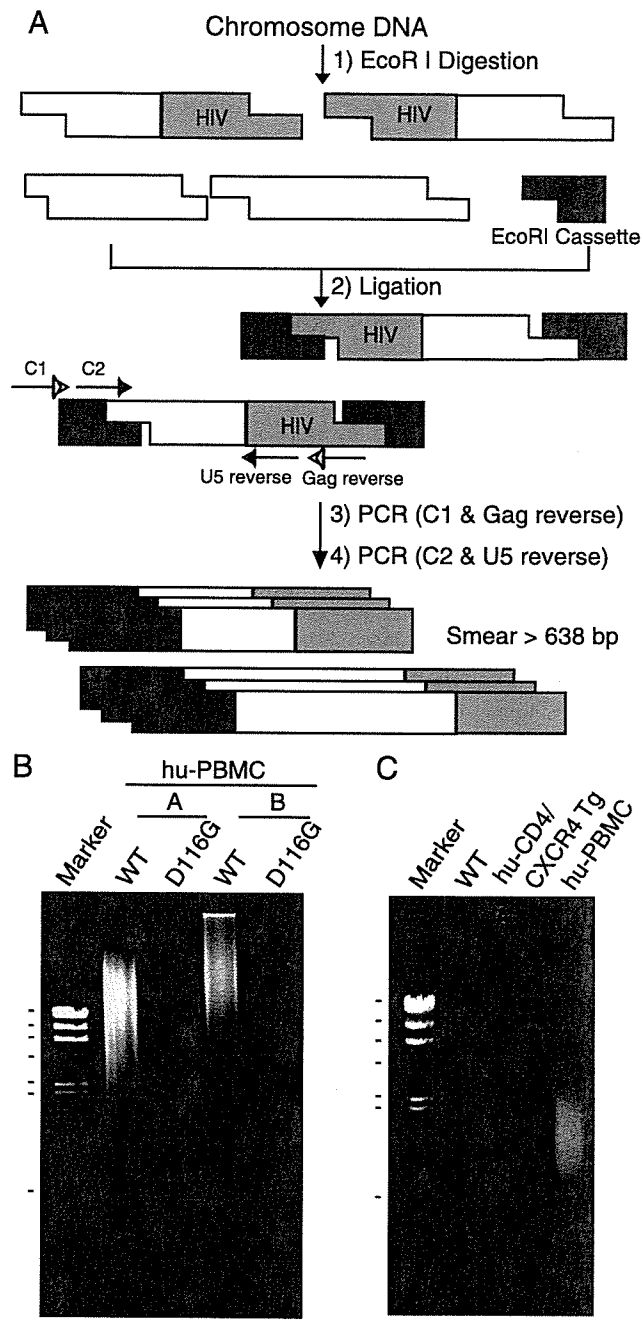

FIG. 3. Suppression of NL4-3 virus DNA integration in the mouse chromosome. Human PBMCs and murine splenocytes were infected with equivalent doses of DNase-treated NL4-3 virus. After 6 h, the virus was removed and the cells were washed with growth medium. At 1 day postinfection, the cells were harvested and used to extract total DNA. The DNA (5 μg) was digested with EcoRI and ligated to double-stranded DNA cassettes with compatible ends. The cassette-ligated DNA fragments were used as templates for nested PCR using cassette- and HIV-specific primers. (A) Schematic representation of cassette ligation-mediated PCR and the primers used to detect HIV integration into the host chromosome. (B and C) Detection of the chromosome-integrated forms of viral DNA. (B) Human PBMC preparations from two donors (A and B) were infected with NL4-3-WT or integrase mutant (D116G), and the DNAs were subjected to PCR analysis. Markers: 23.1, 9.4, 6.6, 4.3, 2.3, 2.0, and 0.564 kb (λ/HindIII). (C) DNA was isolated from NL4-3-infected splenocytes or thymocytes from WT or Tg mice or human PBMCs following infection and subjected to PCR analysis. Note the smearing bands in virus-infected human PBMCs but not in huCD4/CXCR4 Tg mice. Marker: λ/HindIII.

the original length between C2 and U5 reverse primers without insertion. Smearing bands were clearly detected when the DNA from HIV-1 wild type (WT)-infected human PBMCs was analyzed. In contrast, no smearing bands were detected with the DNA from HIV-1-D116G infected human PBMC, HIV-1-WT infected splenocytes from WT, and huCD4/CXCR4 transgenic mice (Fig. 3B and C). These results suggest that HIV-1 replication is also blocked in mouse cells at steps between the entry and viral DNA integration steps or at the viral integration step in addition to the adhesion/entry step.

The infection of mouse cells with both HIV-1/pJD-1 and HIV-1/VSV-G pseudotyped virus are blocked at a postentry step. To examine the possibility that HIV-1 replication in mouse cells is blocked at steps between the viral entry and DNA integration steps, we analyzed the early steps of viral infection using HIV-1 pseudotyped viruses in which the Env is replaced by an amphotropic MuLV Env (HIV-1/pJD-1) or by the G protein of VSV (HIV-1/VSV-G) and the *nef* gene is replaced by the firefly luciferase gene (76). The MuLV envelope pseudotype uses a ubiquitously expressed phosphate transporter as the receptor (55), and the VSV-G envelope pseudotype is capable of infecting cells through a carbohydrate receptor and the endocytic pathway (2). By using these pseudotyped viruses, we overcame the barriers at the adhesion and entry steps.

Among the adherent cells tested, 293T and HeLa cells showed high luciferase activity upon infection with both types of pseudotyped viruses, whereas NIH 3T3 cells yielded 10- to 100-fold-lower signals (Fig. 4). Similarly, the mouse T-cell lines BW5147, EL4, and YAC-1 displayed 100- to 1,000-fold-lower signals than did the human T-cell lines MT4 and Jurkat. Furthermore, luciferase expression efficiency was lower, by more than 1,000-fold, in mouse primary splenocytes than in human PBMCs. The relative sensitivity to infection of these cells was similar between the two pseudotyped viruses, although the efficiency of infection was approximately 10-fold higher in the HIV-1/VSV-G infection. Thus, these results again support a species-specific block in mouse cells subsequent to the entry step.

Reverse transcription of HIV-1 proceeds normally in mouse cells. We next evaluated the ability of mouse cells to support HIV-1 DNA synthesis. One day after infection, total DNA was harvested from various infected cells and subjected to quantitative PCR analyses. Both early (R-U5) and late (R-gag) reverse transcription products were specifically detected in DNA isolated from human and mouse cells exposed to both of the pseudotyped viruses, HIV-1/pJD-1 (Fig. 5A) and HIV-1/VSV-G (Fig. 5B). No R-U5 or R-gag products were detected when heat-inactivated (65°C, 1 h) viruses were infected, indicating that these products were not derived from the transfected HIV-1 DNA carryover. The copy number of R-U5, which reflects the efficiency of viral entry, was higher in mouse cells (NIH 3T3, BW5147, and splenocytes) than in human cells (HeLa, MT4, and PBMCs). The ratio of R-gag/R-U5 was calculated to evaluate the efficiency of the reverse transcription because R-U5 reflects the efficiency of entry (Fig. 5A and B, lower panels). No significant difference in the efficiency of reverse transcription was observed between mouse cells and human cells exposed to HIV-1/pJD-1 (Fig. 5A) and HIV-1/VSV-G (Fig. 5B). These results indicated that mouse cells supported reverse transcription at an efficiency similar to that of human cells.

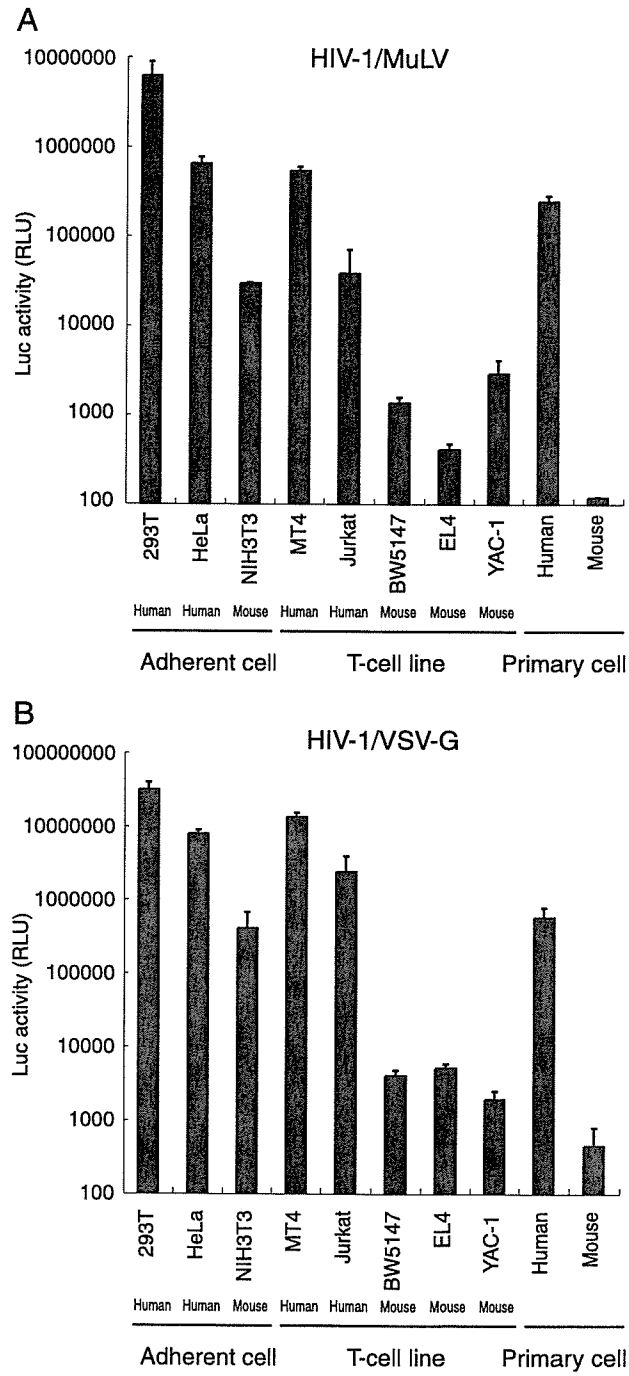

FIG. 4. Analysis of HIV-1 pseudotype virus replication in mouse cells. Human and murine cells were infected with equivalent doses of pNL43lucΔenv that was pseudotyped with either MuLV (A) or VSV-G (B) at 37°C for 6 h. After removal of the virus, cells were washed in growth medium. Luciferase activity was measured at 4 days postinfection, and normalized activities relative to the total protein quantity are shown. The data represent the means ± SEM of results from three wells. The data were reproduced in three independent experiments.

Nuclear import of the PIC is blocked in mouse cells. After completion of reverse transcription, the PIC crosses the

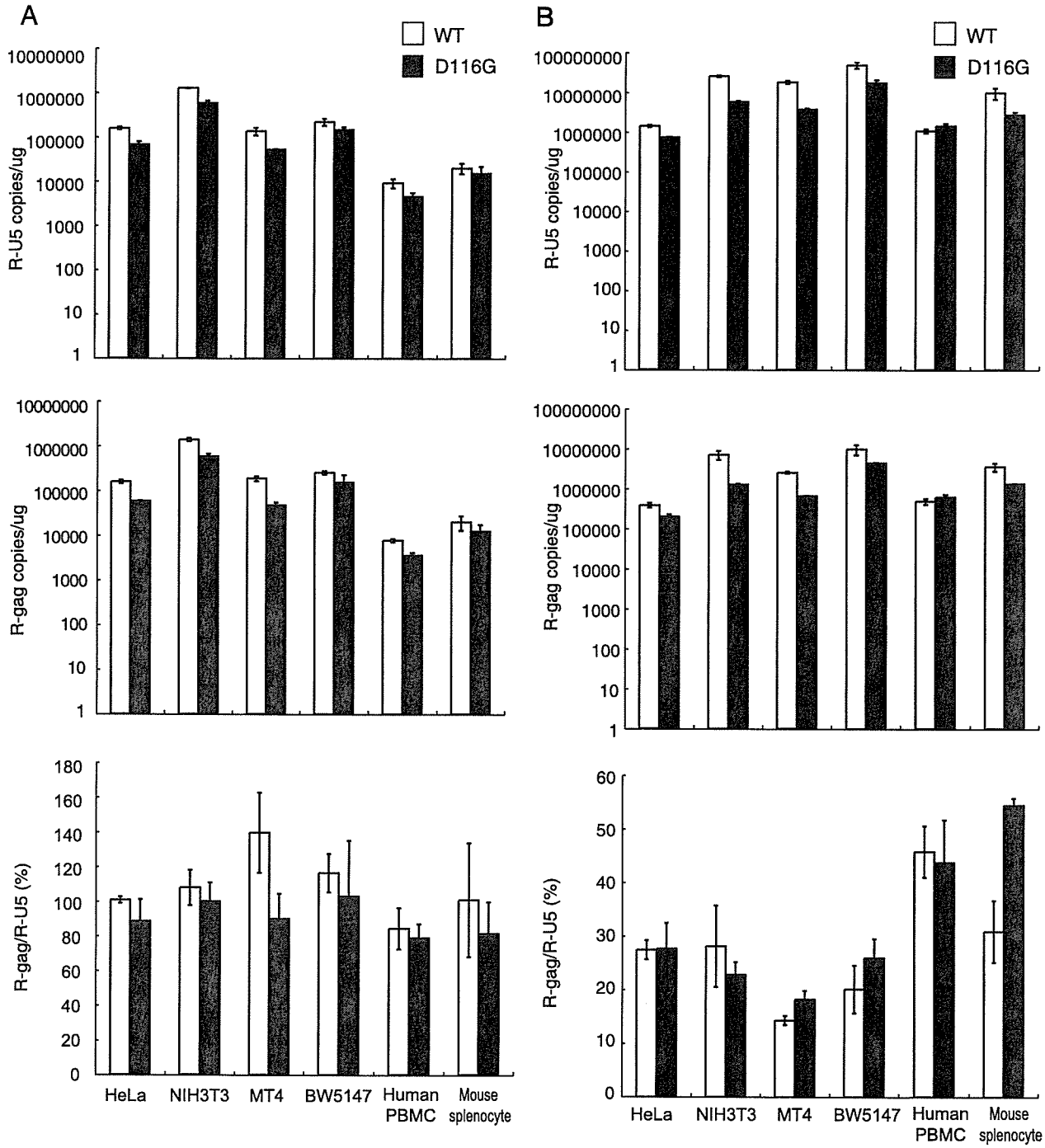

FIG. 5. The efficiency of the reverse transcription of HIV-1 in mouse cells. Human and murine cells were infected with equivalent doses of DNase-treated WT or integrase mutant (D116G) MuLV pseudotyped virus (A) or VSV-G pseudotyped virus (B). At 1 day postinfection, the cells were harvested, and the total DNA was extracted and subjected to quantitative real-time PCR analysis using primer pairs for R/U5 (upper panels) or R/gag (middle panels). The copy numbers of HIV-1 DNA per 1 μg β-actin are shown. The reverse transcription (RT) efficiency is calculated by dividing the late RT product (R-gag) by the early RT product (R-U5) (lower panel). The data represent the means ± SEM of results from three wells. The data were reproduced in three independent experiments.

nuclear membrane and enters the nucleus. Ligases within the nucleus then circularize the proviral DNA (2-LTR containing circular DNA) before its integration into the host chromosome (17, 57, 82). Although these 2-LTR circles are nonfunctional, they can serve as a measure of viral nuclear entry. To assess the efficiency of PIC transport into the nuclei of mouse cells, we estimated de novo-synthesized 2-LTR circular-form DNA by PCR using primer pairs that amplify sequences unique to this DNA form. The fragment corresponding to the 2-LTR circular junction was clearly

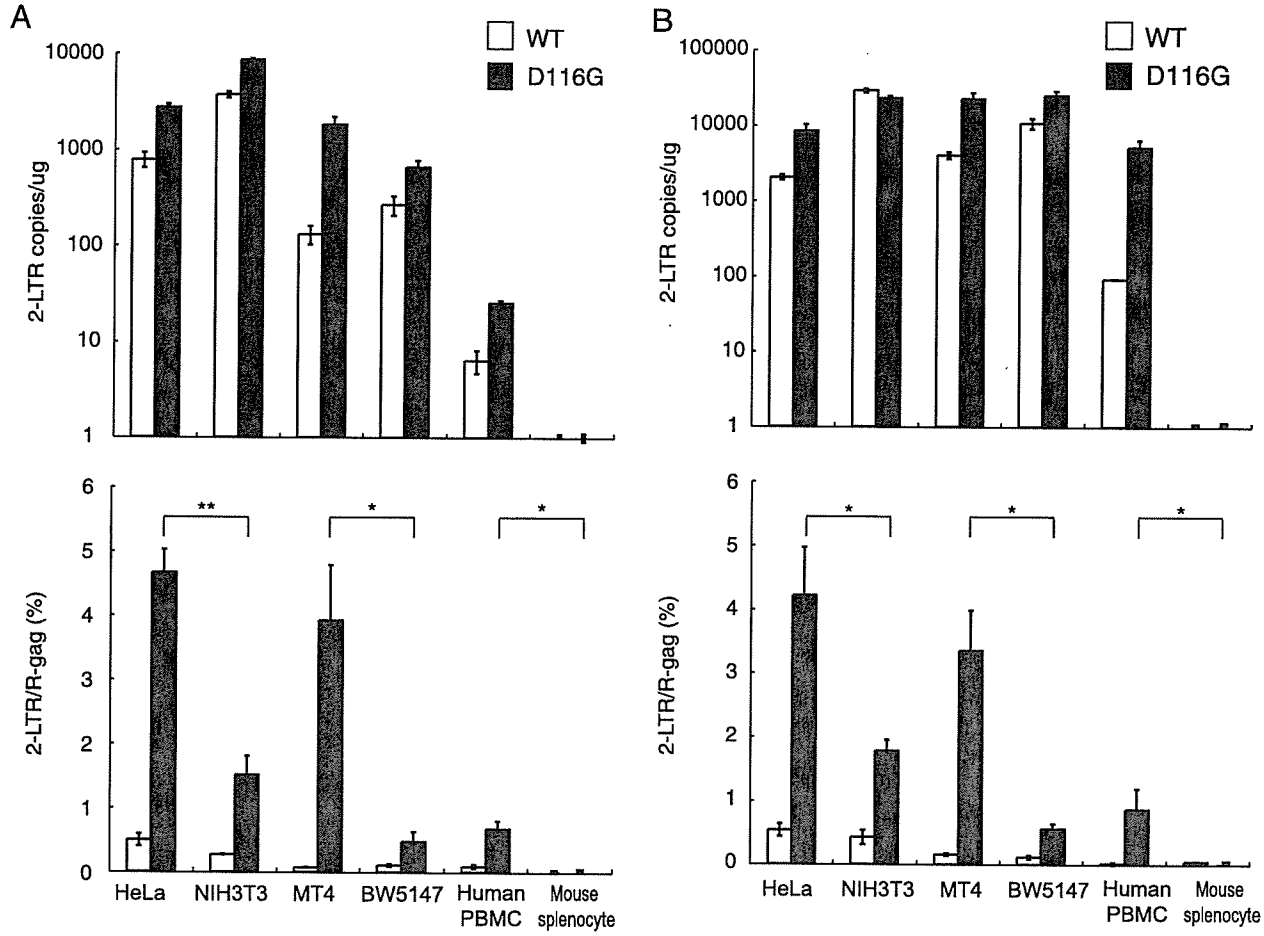

FIG. 6. Suppression of the 2-LTR circular form of DNA in mouse cells. Human and mouse cells were infected with equivalent doses of DNase-treated WT or integrase-mutant (D116G) MuLV pseudotype virus (A) or VSV-G pseudotype virus (B). The DNA from the infected cells was subjected to quantitative real-time PCR analysis using a primer pair specific for the 2-LTR circular form of the DNA (upper panels). The nuclear import efficiency was calculated by dividing the 2-LTR products by the late reverse transcription products (lower panels). The data represent the means ± SEM of results from three wells, and the data were reproduced in three independent experiments. *, $P < 0.05$; **, $P < 0.01$ (determined by Student's t test).

detected at 1 day postinfection in the DNA samples from HeLa, NIH 3T3, MT-4, BW5147, and human PBMCs infected with HIV-1/pJD-1 pseudotyped virus (Fig. 6A, upper panel). However, only a small amount of 2-LTR circle was detected in the mouse splenocytes. A similar tendency was observed in cells infected with the HIV-1/VSV-G pseudotyped virus (Fig. 6B, upper panel). The 2-LTR DNA in mouse cells was also measured at 2 and 4 days postinfection using both pseudotyped viruses and provided similar results (data not shown).

The ratio of 2-LTR/R-gag was calculated to evaluate the efficiency of nuclear import because the copy number of 2-LTR in the nucleus should be dependent on the amount of cytoplasmic R-gag, which represents the precursor of 2-LTR. The efficiency was very low and not significantly different between human and mouse when wild-type HIV-1 pseudovirus was infected (Fig. 6, lower panel). Because the nuclear concentration of 2-LTR is determined by the balance between accumulation of PIC by nuclear import and loss of PIC from the nucleoplasm by chromosome integration, we next used an integration-defective mutant, D116G, to examine only the efficiency of nuclear import. As shown in Fig. 6, the ratio was significantly lower in NIH 3T3 cells than in HeLa cells (33% or 43% of HeLa cells) and in BW5147 cells than in MT4 cells (12% or 17% of MT4 cells) when they were infected with HIV-1/pJD-1 or HIV-1/VSV-G, respectively (Fig. 6A and B, lower panels). We were unable to compare the efficiency of PIC import in human PBMCs and mouse splenocytes because the 2-LTR circle was not detected in mouse splenocytes. These results suggested that the nuclear import of the PIC is blocked in mouse cells, especially in splenocytes.

A block in the nuclear localization of the PIC is caused by a defect in IN nuclear localization. As Vpr and IN play important roles in importing the PIC into the nucleus, we hypothesized that Vpr and/or IN is nonfunctional in mouse cells due to the inability to utilize the cellular factors necessary for trafficking to the nucleus. To directly examine the karyophilic properties of HIV-1 IN in mouse cells, we generated an expression vector with HIV-1 IN in which the N terminus was fused to EGFP (GFP-IN). Since it was reported that β-galactosidase fusion to the C terminus of IN could not be located in

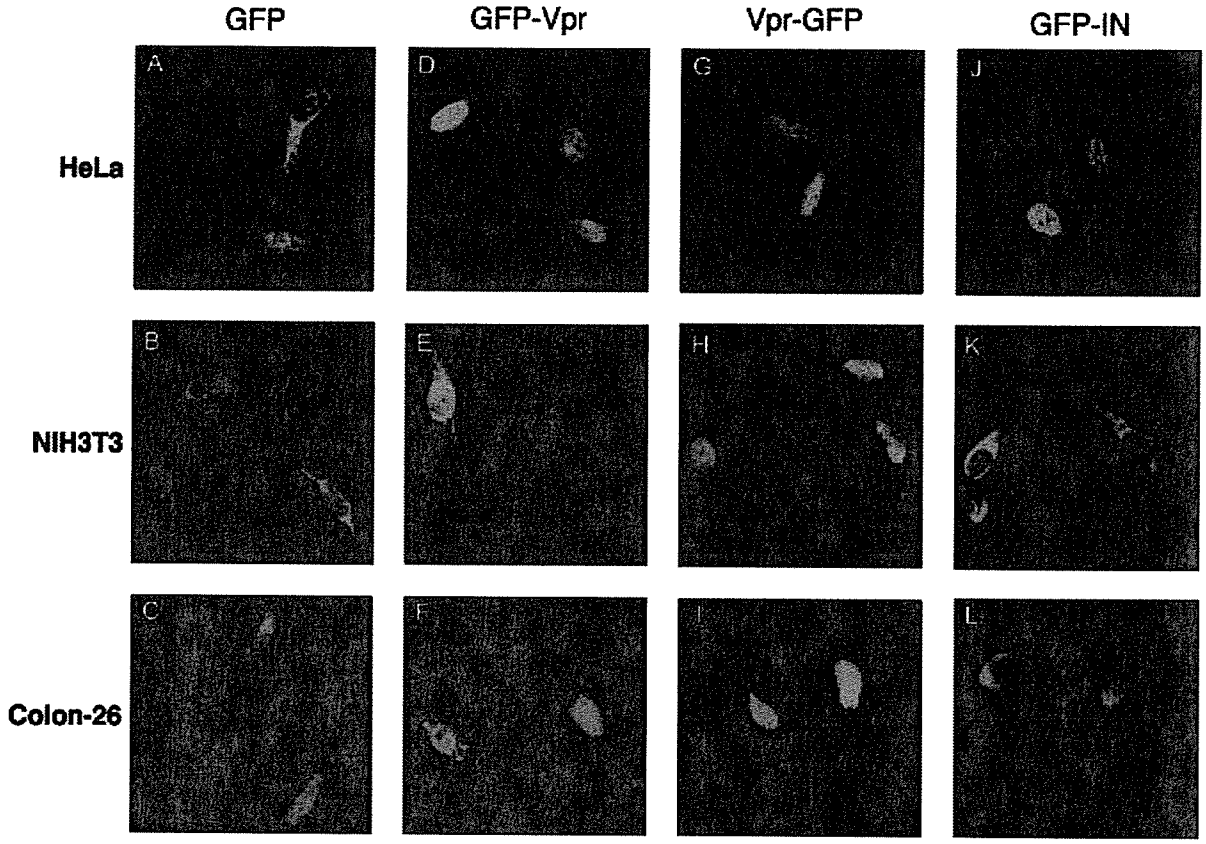

FIG. 7. Inhibition of IN-dependent GFP nuclear import in mouse cells. HeLa (A, D, G, and J), NIH 3T3 (B, E, H, and K), and Colon-26 cells (C, F, I, and L) were transfected with plasmids expressing GFP only (A, B, and C), GFP fused to the HIV-1 Vpr N terminus (GFP-Vpr) (D, E, and F), GFP fused to the HIV-1 Vpr C terminus (Vpr-GFP) (G, H, and I), and GFP fused to HIV-1 IN (J, K, and L) using Lipofectamine 2000. At 24 h posttransfection, the cells were fixed and visualized by confocal fluorescence microscopy. Note that the nuclear localization of GFP-IN is inhibited in mouse cells (K and L).

the nucleus (44), we did not examine the C terminus fusion construct (IN-GFP). We also generated HIV-1 Vpr expression vectors in which the N or C terminus was fused to EGFP (GFP-Vpr and Vpr-GFP, respectively). At 24 h postinfection, HeLa, NIH 3T3, and Colon-26 cells were transfected with the GFP fusion vectors, and the subcellular localization of IN or Vpr was examined with a confocal microscope. We used Colon-26 cells (Fv-1^n) in addition to NIH 3T3 cells (Fv-1^b) because Fv-1 may exert its antiretroviral effect at a postentry step, after reverse transcription and prior to integration (38, 79). Colon-26 cells and NIH 3T3 cells showed similar levels of luciferase activity upon infection with both types of pseudotyped viruses. Control GFP without IN or Vpr was distributed uniformly throughout both the cytoplasm and the nuclei in all cells examined (Fig. 7A to C). GFP-Vpr, on the other hand, accumulated almost exclusively in the nuclei of HeLa (Fig. 7D), NIH 3T3 (Fig. 7E), and Colon-26 (Fig. 7F) cells, although low levels of nuclear membrane association were also observed in NIH 3T3 cells (Fig. 7E). Vpr-GFP also accumulated almost exclusively in the nuclei of HeLa (Fig. 7G), NIH 3T3 (Fig. 7H), and Colon-26 (Fig. 7I) cells. These results indicated that HIV-1 Vpr has strong karyophilic properties and that, even in mouse cells, it can be transported across the nuclear membrane. In contrast, although GFP-IN accumulated almost exclusively in the nuclei of HeLa cells (Fig. 7J), GFP-IN was localized only in the cytoplasm of NIH 3T3 (Fig. 7K) and Colon-26 (Fig. 7L) cells. Thus, our results demonstrate that IN-mediated nuclear transport of HIV-1 PIC is impaired in mouse cells of both Fv-1 genotypes.

Addition of the SV40 NLS to the C terminus of HIV-1 integrase enhances viral infectivity in mouse cells. To analyze the role of IN in nuclear localization of HIV-1, we constructed an HIV-1 pNL43lucΔenv vector with the SV40 NLS at the C terminus of IN (IN-NLS), and pseudotyped virus was generated by cotransfection of 293T cells with the pNL43lucΔenv wild type or IN-NLS vector and VSV-G expression vector. Luciferase activity in the cell lysate of 293T cells transfected with IN-NLS was increased 2.5-fold compared to that transfected with wild-type virus (Fig. 8A). To verify that the gag-pol polyprotein processing was completed in IN-NLS virus particles, we performed Western blot analysis using an AIDS patient serum. No difference of the viral components was observed between parental WT and IN-NLS viruses (Fig. 8B). The content of p24 protein of the IN-NLS was also shown to be normal using a specific monoclonal antibody (data not shown). These results showed that addition of NLS to IN significantly activates viral replication.

Then we tested the susceptibility of HeLa, NIH 3T3, BW5147, and MT4 cells to IN-NLS infection. Addition of the

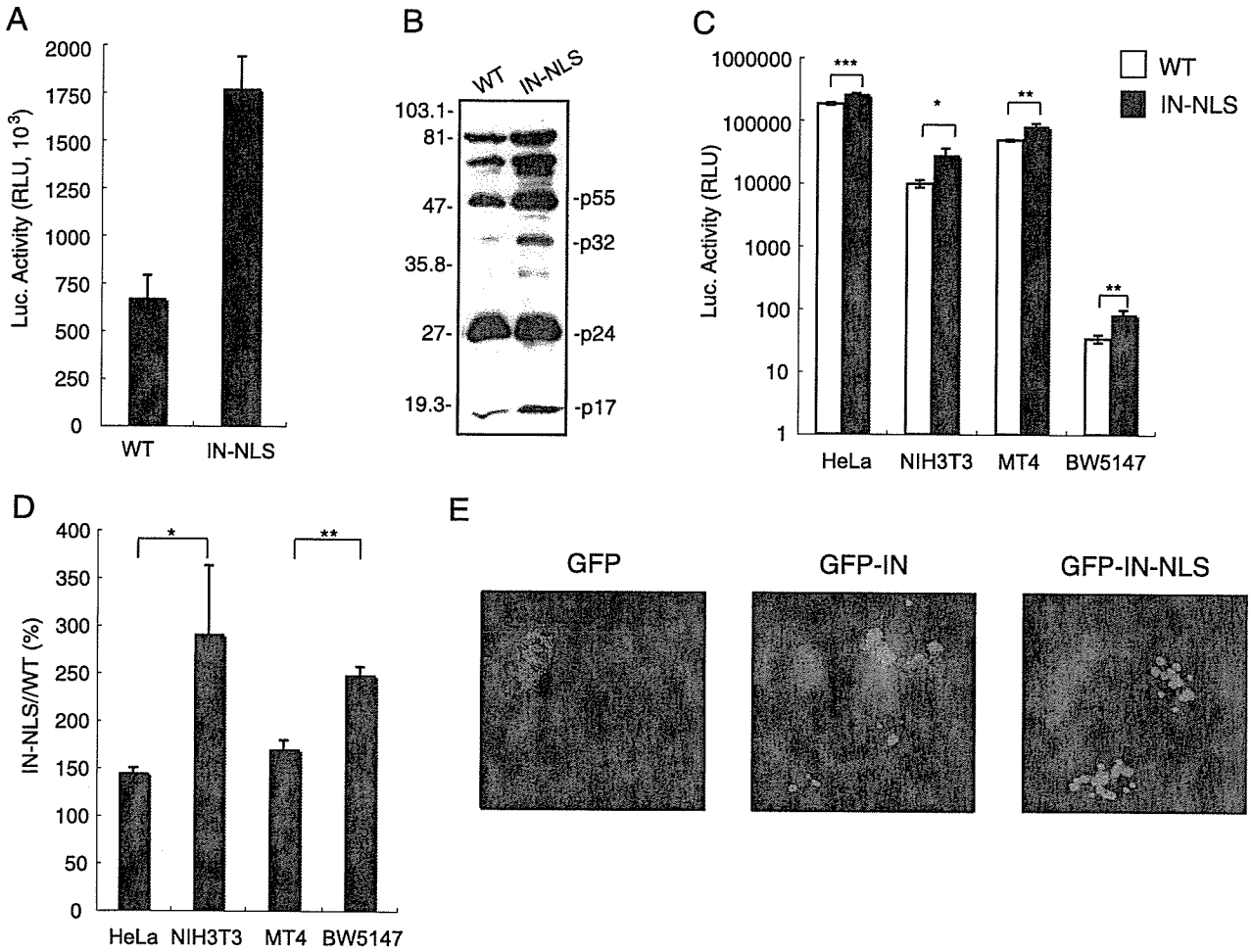

FIG. 8. Enhancement of viral infectivity to mouse cells by the addition of SV40 NLS to the C terminus of IN. (A) Luciferase activity in an HIV-1 pNL43lucΔenv vector (WT) or pNL43lucΔenv vector carrying an SV40 NLS-ligated IN (IN-NLS)-transfected 293T cells were measured at 2 days posttransfection. The data were reproduced in 10 independent experiments. (B) Virus particles were collected at 48 h posttransfection and resuspended in PBS. The viral pellets were hearted at 90°C for 10 min in the presence of sample buffer (62.5 mM Tris-HCl, pH 6.8, 10% glycerol, 2% SDS, 5% 2-mercaptoethanol, 0.005% bromophenol blue). Then viral proteins were electrophoresed on a 12% SDS–polyacrylamide gel. Viral proteins were detected with AIDS patient serum. Positions of the major viral proteins are indicated together with molecular weight markers. (C) Human and mouse cells were infected with equivalent amounts of WT (□) or IN-NLS (■) virus at 37°C for 6 h, and then the virus was removed. The luciferase activity was measured 4 days after infection, and the activity was normalized relative to the total amount of protein. Means ± SEM are shown. (D) Relative Luc activities of IN-NLS virus-infected cells compared to WT virus-infected cells were calculated using the data shown in panel C. Means ± SEM are shown. (E) NIH 3T3 cells transfected with a plasmid expressing GFP, GFP-IN, or GFP-IN-NLS fusion protein were analyzed by confocal microscopy. At 24 h posttransfection, cells were fixed and GFP was detected by a confocal fluorescent microscope. *, $P < 0.05$; **, $P < 0.01$; ***, $P < 0.001$ (by Student's t test).

SV40 NLS to the C terminus of IN significantly enhanced viral infectivity in all cell lines used (Fig. 8C). As the NLS fusion at the C terminus of IN disrupted the *vif* gene, we did not analyze the infectivity to human PBMC, which was nonpermissive to *vif*-deficient virus (24, 69). Interestingly, the effect of the NLS on viral infection was significantly stronger in mouse cells than in human cells (Fig. 8D).

We also analyzed the karyophilic property of GFP-IN-NLS in which EGFP was fused to the N terminus and the SV40 NLS at the C terminus of IN. GFP-IN-NLS accumulated almost exclusively in the nucleus of NIH 3T3 cells, in contrast to GFP-IN (Fig. 8E). These results indicate that the addition of functional NLS to IN compensates the functional defects of IN in mouse cells.

DISCUSSION

HIV-1 replication in rodent cells is blocked at multiple steps, including viral entry, transcription, nuclear export of the mRNA, assembly, and budding (77). In this study, we demonstrated that an additional host range barrier is present in mouse cells at the PIC nuclear transport step. We suggest that this restriction is caused by the dysfunction of the HIV-1 IN-dependent PIC import system.

We found that the ratio of the 2-LTR circular product to the late reverse transcription product (R-gag), which are produced in the nucleus and cytoplasm, respectively, was decreased in mouse splenocytes relative to human PBMCs after infection with both HIV-1/MuLV and HIV-1/VSV-G pseudotyped vi-

ruses (Fig. 6, lower panels). This indicates a reduction in nuclear import of the PIC. The efficiency of nuclear transfer of the viral PIC was recently reported to be reduced in mouse T cells relative to human T cell lines, but not in NIH 3T3 cells (7). These results are consistent with ours, although we cannot explain their lack of reduction in the NIH 3T3 cells. Our system using the IN mutant virus is probably more sensitive in detecting the defect.

We showed that the infection efficiency, as determined by luciferase activity, was 10 to 100, 100 to 1,000, and >1.000 times lower than in human cells in mouse adherent cells, T cell lines, and primary cells, respectively (Fig. 4). As the PIC nuclear import reduction in mouse cells was at most 60 to 90% compared to human cells (Fig. 6), it is clear that other barriers are also involved in the HIV-1 replication restriction in mouse cells. In this regard, we showed that the 2-LTR/R-gag ratio following infection with WT HIV-1 was similar between HeLa and NIH 3T3 cells and between MT4 and BW5147 cells, in contrast to our observations with the IN-deficient mutant virus (Fig. 6, lower panels). These results are explainable if the R-gag products integrate rapidly into the host chromosome in human cells compared to mouse cells, assuming that a constant proportion of free R-gag products is converted into the 2-LTR form. Thus, integration of the R-gag products into the host chromosome may also be inhibited in mouse cells. In accordance with this idea, we demonstrated that the integration frequency of HIV-1 was greatly reduced upon infection with WT HIV-1 in mouse cells transgenic for the huCD4/CXCR4 genes.

There are two formal explanations for the inability of the mouse cells to support HIV-1 PIC nuclear import. One is the absence of a required human-specific factor, and the other is the presence of an inhibitory factor(s) in mouse cells. However, because mouse-human cell fusions allow viral replication, mouse cells most likely do not have such an inhibitory factor and are rather devoid of a critical factor for the import of the HIV-1 PIC (52).

Although the mechanisms of PIC nuclear import have not been elucidated completely, NLSs are present in three viral proteins (MA, Vpr, and IN) as well as in a central DNA flap produced during reverse transcription that also contributes to the successful nuclear targeting of the PIC (59, 64, 71). Although their respective contributions remain controversial and unclear, it has been clearly shown that both Vpr and IN are karyophilic and rapidly accumulate in the nuclei of infected cells (6, 16, 19, 20, 25, 32, 48, 63, 66, 68). Meanwhile, localization of MA to the nucleus is not well established (14, 23). In this report, we demonstrated that GFP-fused IN remained in the cytoplasm of NIH 3T3 cells, in contrast to its accumulation in the nuclei of HeLa cells. On the other hand, when GFP-fused Vprs were examined, they localized to the nuclei of both NIH 3T3 and HeLa cells. The nuclear distribution of GFP-IN, but not GFP-fused Vpr, was also inhibited in the Colon-26 mouse cell line. These observations indicate that Vpr can be imported into the nucleus using separate pathways. IN, on the other hand, cannot be imported efficiently into the nuclei of mouse cells, and this is probably due to the inability of IN to interact with mouse nuclear import system.

In support for this notion, we showed that nuclear import of IN was much more enhanced in mouse cells than in human cells when authentic SV40 NLS was added to IN (Fig. 8). Furthermore, the addition of this NLS to IN significantly enhanced the infectivity of HIV-1 pseudovirus to mouse cells. These results indicate that endogenous nuclear localization signals of IN are not fully functional in mouse cells.

In this context, it is known that the NLSs within HIV-1 IN are composed of basic amino acid-rich sequences that interact with importin β through the adapter importin (25). We previously showed, however, that mutational disruption of the suggested NLSs could not abolish the nuclear localization of a GFP-IN fusion protein (76). Recent studies have shown that nonclassical NLSs are necessary and sufficient to locate the viral PIC into the nuclei (12). Depienne et al. suggested that the in vitro nuclear import of IN does not require known cytosolic transport factors, including karyopherin β family proteins (18). Two proteins have recently been reported to mediate PIC import. The first is lens epithelium-derived growth factor (LEDGF/p75), a protein implicated in the regulation of gene expression and cellular stress responses. LEDGF interacts with HIV-1 IN in vitro and in living cells (50) and colocalizes with HIV-IN in the nuclei of human cells (15). The second is importin 7, a mildly hydrophobic protein belonging to the importin β superfamily. This protein is suggested to interact with basic proteins, such as IN, that bind viral nucleic acids (21). It is currently unclear which protein(s) is important in these processes and defective in mouse cells. Clearly, further work is necessary to identify the host cell factors that are associated with IN in human cells and defective in mouse cells.

Thus far, several host restriction factors are known to be involved in the suppression of HIV-1 replication in the early phase of its life cycle in mouse cells. Friend virus susceptibility factor-1 (Fv-1) is involved in the restriction of specific mouse cell genotypes to MuLV (10, 28). The Fv-1 targets the MuLV capsid and stops the nuclear import of the PIC (8, 39). However, recent reports have noted that there is no correlation between HIV-1 susceptibility and cellular Fv-1 genotype (7, 31). Tripartite motif 5 α (TRIM5α), encoded by the gene *Lv-1*, is another restriction factor (72). TRIM5α inhibits viral replication in rhesus macaque cells at a step after entry but before the reverse transcription of HIV-1 by targeting the viral capsid protein (60). Thus, both Fv-1 and TRIM5α function in processes other than the transport of PIC into the nucleus.

In conclusion, we have demonstrated that PIC nuclear import is blocked in mouse cells and that dysfunctional IN is at least partially responsible for the barrier. Further characterization and identification of factors that are involved in PIC nuclear import should provide new insight into the molecular mechanisms of the PIC import step and clues to the development of new therapeutics. Furthermore, identification of the factors responsible for this step will assist in our generation of transgenic small animal models that are permissive to HIV-1 infection.

ACKNOWLEDGMENTS

We thank Takao Masuda (Tokyo Dental and Medical University) for providing pNL43lucΔenv and an amphotropic Moloney MuLV envelope expression vector (pJD-1) as well as for critical discussions. We also thank Yoshio Koyanagi (Kyoto University) for providing the 2-LTR plasmid and the AIDS patient serum and for important technical advice. We also thank Yoshio Inagaki (Tokyo Medical and Dental University) for providing the AIDS patient serum. We are grateful

to Luigi Naldini (San Raffaele Telethon Institute for Gene Therapy) and Kenzaburo Tani (Kyushu University) for providing the VSV-G envelope-expressing plasmid (pMD-G).

This work was supported by Grants-in-Aid from the Japan Human Sciences Foundation.

REFERENCES

1. **Adachi, A., H. E. Gendelman, S. Koenig, T. Folks, R. Willey, A. Rabson, and M. A. Martin.** 1986. Production of acquired immunodeficiency syndrome-associated retrovirus in human and nonhuman cells transfected with an infectious molecular clone. J. Virol. **59:**284–291.
2. **Aiken, C.** 1997. Pseudotyping human immunodeficiency virus type 1 (HIV-1) by the glycoprotein of vesicular stomatitis virus targets HIV-1 entry to an endocytic pathway and suppresses both the requirement for Nef and the sensitivity to cyclosporin A. J. Virol. **71:**5871–5877.
3. **Alonso, A., T. P. Cujec, and B. M. Peterlin.** 1994. Effects of human chromosome 12 on interactions between Tat and TAR of human immunodeficiency virus type 1. J. Virol. **68:**6505–6513.
4. **Alonso, A., D. Derse, and B. M. Peterlin.** 1992. Human chromosome 12 is required for optimal interactions between Tat and TAR of human immunodeficiency virus type 1 in rodent cells. J. Virol. **66:**4617–4621.
5. **Bai, Y., Y. Soda, K. Izawa, T. Tanabe, X. Kang, A. Tojo, H. Hoshino, H. Miyoshi, S. Asano, and K. Tani.** 2003. Effective transduction and stable transgene expression in human blood cells by a third-generation lentiviral vector. Gene Ther. **10:**1446–1457.
6. **Balliet, J. W., D. L. Kolson, G. Eiger, F. M. Kim, K. A. McGann, A. Srinivasan, and R. Collman.** 1994. Distinct effects in primary macrophages and lymphocytes of the human immunodeficiency virus type 1 accessory genes vpr, vpu, and nef: mutational analysis of a primary HIV-1 isolate. Virology **200:**623–631.
7. **Baumann, J. G., D. Unutmaz, M. D. Miller, S. K. Breun, S. M. Grill, J. Mirro, D. R. Littman, A. Rein, and V. N. KewalRamani.** 2004. Murine T cells potently restrict human immunodeficiency virus infection. J. Virol. **78:**12537–12547.
8. **Benit, L., N. De Parseval, J. F. Casella, I. Callebaut, A. Cordonnier, and T. Heidmann.** 1997. Cloning of a new murine endogenous retrovirus, MuERV-L, with strong similarity to the human HERV-L element and with a gag coding sequence closely related to the Fv1 restriction gene. J. Virol. **71:**5652–5657.
9. **Berson, J. F., D. Long, B. J. Doranz, J. Rucker, F. R. Jirik, and R. W. Doms.** 1996. A seven-transmembrane domain receptor involved in fusion and entry of T-cell-tropic human immunodeficiency virus type 1 strains. J. Virol. **70:**6288–6295.
10. **Best, S., P. Le Tissier, G. Towers, and J. P. Stoye.** 1996. Positional cloning of the mouse retrovirus restriction gene Fv1. Nature **382:**826–829.
11. **Bieniasz, P. D., and B. R. Cullen.** 2000. Multiple blocks to human immunodeficiency virus type 1 replication in rodent cells. J. Virol. **74:**9868–9877.
12. **Bouyac-Bertoia, M., J. D. Dvorin, R. A. Fouchier, Y. Jenkins, B. E. Meyer, L. I. Wu, M. Emerman, and M. H. Malim.** 2001. HIV-1 infection requires a functional integrase NLS. Mol. Cell **7:**1025–1035.
13. **Browning, J., J. W. Horner, M. Pettoello-Mantovani, C. Raker, S. Yurasov, R. A. DePinho, and H. Goldstein.** 1997. Mice transgenic for human CD4 and CCR5 are susceptible to HIV infection. Proc. Natl. Acad. Sci. USA **94:**14637–14641.
14. **Bukrinsky, M., K. Manogue, and A. Cerami.** 1995. HIV results in the frame. Other approaches. Nature **375:**195–196. (Author's reply, **375:**198.)
15. **Cherepanov, P., G. Maertens, P. Proost, B. Devreese, J. Van Beeumen, Y. Engelborghs, E. De Clercq, and Z. Debyser.** 2003. HIV-1 integrase forms stable tetramers and associates with LEDGF/p75 protein in human cells. J. Biol. Chem. **278:**372–381.
16. **Connor, R. I., B. K. Chen, S. Choe, and N. R. Landau.** 1995. Vpr is required for efficient replication of human immunodeficiency virus type-1 in mononuclear phagocytes. Virology **206:**935–944.
17. **Cullen, B. R.** 2001. Journey to the center of the cell. Cell **105:**697–700.
18. **Depienne, C., A. Mousnier, H. Leh, E. Le Rouzic, D. Dormont, S. Benichou, and C. Dargemont.** 2001. Characterization of the nuclear import pathway for HIV-1 integrase. J. Biol. Chem. **276:**18102–18107.
19. **Depienne, C., P. Roques, C. Creminon, L. Fritsch, R. Casseron, D. Dormont, C. Dargemont, and S. Benichou.** 2000. Cellular distribution and karyophilic properties of matrix, integrase, and Vpr proteins from the human and simian immunodeficiency viruses. Exp. Cell Res. **260:**387–395.
20. **Farnet, C. M., B. Wang, J. R. Lipford, and F. D. Bushman.** 1996. Differential inhibition of HIV-1 preintegration complexes and purified integrase protein by small molecules. Proc. Natl. Acad. Sci. USA **93:**9742–9747.
21. **Fassati, A., D. Gorlich, I. Harrison, L. Zaytseva, and J. M. Mingot.** 2003. Nuclear import of HIV-1 intracellular reverse transcription complexes is mediated by importin 7. EMBO J. **22:**3675–3685.
22. **Feng, Y., C. C. Broder, P. E. Kennedy, and E. A. Berger.** 1996. HIV-1 entry cofactor: functional cDNA cloning of a seven-transmembrane, G protein-coupled receptor. Science **272:**872–877.
23. **Fouchier, R. A., B. E. Meyer, J. H. Simon, U. Fischer, and M. H. Malim.** 1997. HIV-1 infection of non-dividing cells: evidence that the amino-terminal basic region of the viral matrix protein is important for Gag processing but not for post-entry nuclear import. EMBO J. **16:**4531–4539.
24. **Gabuzda, D. H., H. Li, K. Lawrence, B. S. Vasir, K. Crawford, and E. Langhoff.** 1994. Essential role of vif in establishing productive HIV-1 infection in peripheral blood T lymphocytes and monocyte/macrophages. J. Acquir. Immune Defic. Syndr. **7:**908–915.
25. **Gallay, P., T. Hope, D. Chin, and D. Trono.** 1997. HIV-1 infection of nondividing cells through the recognition of integrase by the importin/karyopherin pathway. Proc. Natl. Acad. Sci. USA **94:**9825–9830.
26. **Garber, M. E., and K. A. Jones.** 1999. HIV-1 Tat: coping with negative elongation factors. Curr. Opin. Immunol. **11:**460–465.
27. **Garber, M. E., P. Wei, V. N. KewalRamani, T. P. Mayall, C. H. Herrmann, A. P. Rice, D. R. Littman, and K. A. Jones.** 1998. The interaction between HIV-1 Tat and human cyclin T1 requires zinc and a critical cysteine residue that is not conserved in the murine CycT1 protein. Genes Dev. **12:**3512–3527.
28. **Goff, S. P.** 1996. Operating under a Gag order: a block against incoming virus by the Fv1 gene. Cell **86:**691–693.
29. **Habu, K., J. Nakayama-Yamada, M. Asano, S. Saijo, K. Itagaki, R. Horai, H. Yamamoto, T. Sekiguchi, T. Nosaka, M. Hatanaka, and Y. Iwakura.** 1999. The human T cell leukemia virus type I-tax gene is responsible for the development of both inflammatory polyarthropathy resembling rheumatoid arthritis and noninflammatory ankylotic arthropathy in transgenic mice. J. Immunol. **162:**2956–2963.
30. **Hart, C. E., C. Y. Ou, J. C. Galphin, J. Moore, L. T. Bacheler, J. J. Wasmuth, S. R. Petteway, Jr., and G. Schochetman.** 1989. Human chromosome 12 is required for elevated HIV-1 expression in human-hamster hybrid cells. Science **246:**488–491.
31. **Hatziioannou, T., S. Cowan, and P. D. Bieniasz.** 2004. Capsid-dependent and -independent postentry restriction of primate lentivirus tropism in rodent cells. J. Virol. **78:**1006–1011.
32. **Heinzinger, N. K., M. I. Bukinsky, S. A. Haggerty, A. M. Ragland, V. Kewalramani, M. A. Lee, H. E. Gendelman, L. Ratner, M. Stevenson, and M. Emerman.** 1994. The Vpr protein of human immunodeficiency virus type 1 influences nuclear localization of viral nucleic acids in nondividing host cells. Proc. Natl. Acad. Sci. USA **91:**7311–7315.
33. **Ho, S. N., H. D. Hunt, R. M. Horton, J. K. Pullen, and L. R. Pease.** 1989. Site-directed mutagenesis by overlap extension using the polymerase chain reaction. Gene **77:**51–59.
34. **Hogan, B., E. Constantini, and E. Lacey.** 1994. Manipulating the mouse embryo: a laboratory manual, 2nd ed. Cold Spring Harbor Laboratory Press, Cold Spring Harbor, NY.
35. **Isegawa, Y., J. Sheng, Y. Sokawa, K. Yamanishi, O. Nakagomi, and S. Ueda.** 1992. Selective amplification of cDNA sequence from total RNA by cassette-ligation mediated polymerase chain reaction (PCR): application to sequencing 6.5 kb genome segment of hantavirus strain B-1. Mol. Cell Probes **6:**467–475.
36. **Iwakura, Y., T. Shioda, M. Tosu, E. Yoshida, M. Hayashi, T. Nagata, and H. Shibuta.** 1992. The induction of cataracts by HIV-1 in transgenic mice. AIDS **6:**1069–1075.
37. **Jackson, J. B., K. L. MacDonald, J. Cadwell, C. Sullivan, W. E. Kline, M. Hanson, K. J. Sannerud, S. L. Stramer, N. J. Fildes, S. Y. Kwok, et al.** 1990. Absence of HIV infection in blood donors with indeterminate western blot tests for antibody to HIV-1. N. Engl. J. Med. **322:**217–222.
38. **Jolicoeur, P., and D. Baltimore.** 1976. Effect of Fv-1 gene product on proviral DNA formation and integration in cells infected with murine leukemia viruses. Proc. Natl. Acad. Sci. USA **73:**2236–2240.
39. **Jolicoeur, P., and E. Rassart.** 1980. Effect of Fv-1 gene product on synthesis of linear and supercoiled viral DNA in cells infected with murine leukemia virus. J. Virol. **33:**183–195.
40. **Keppler, O. T., W. Yonemoto, F. J. Welte, K. S. Patton, D. Iacovides, R. E. Atchison, T. Ngo, D. L. Hirschberg, R. F. Speck, and M. A. Goldsmith.** 2001. Susceptibility of rat-derived cells to replication by human immunodeficiency virus type 1. J. Virol. **75:**8063–8073.
41. **Klatzmann, D., E. Champagne, S. Chamaret, J. Gruest, D. Guetard, T. Hercend, J. C. Gluckman, and L. Montagnier.** 1984. T-lymphocyte T4 molecule behaves as the receptor for human retrovirus LAV. Nature **312:**767–768.
42. **Koito, A., Y. Kameyama, C. Cheng-Mayer, and S. Matsushita.** 2003. Susceptibility of mink (Mustera vision)-derived cells to replication by human immunodeficiency virus type 1. J. Virol. **77:**5109–5117.
43. **Koito, A., H. Shigekane, and S. Matsushita.** 2003. Ability of small animal cells to support the postintegration phase of human immunodeficiency virus type-1 replication. Virology **305:**181–191.
44. **Kukolj, G., K. S. Jones, and A. M. Skalka.** 1997. Subcellular localization of avian sarcoma virus and human immunodeficiency virus type 1 integrases. J. Virol. **71:**843–847.
45. **Kwok, S., D. E. Kellogg, N. McKinney, D. Spasic, L. Goda, C. Levenson, and J. J. Sninsky.** 1990. Effects of primer-template mismatches on the polymerase chain reaction: human immunodeficiency virus type 1 model studies. Nucleic Acids Res. **18:**999–1005.

46. **Landau, N. R., M. Warton, and D. R. Littman.** 1988. The envelope glycoprotein of the human immunodeficiency virus binds to the immunoglobulin-like domain of CD4. Nature **334**:159–162.
47. **Lores, P., V. Boucher, C. Mackay, M. Pla, H. Von Boehmer, J. Jami, F. Barre-Sinoussi, and J. C. Weill.** 1992. Expression of human CD4 in transgenic mice does not confer sensitivity to human immunodeficiency virus infection. AIDS Res. Hum. Retrovir. **8**:2063–2071.
48. **Lu, Y. L., P. Spearman, and L. Ratner.** 1993. Human immunodeficiency virus type 1 viral protein R localization in infected cells and virions. J. Virol. **67**:6542–6550.
49. **Maddon, P. J., A. G. Dalgleish, J. S. McDougal, P. R. Clapham, R. A. Weiss, and R. Axel.** 1986. The T4 gene encodes the AIDS virus receptor and is expressed in the immune system and the brain. Cell **47**:333–348.
50. **Maertens, G., P. Cherepanov, W. Pluymers, K. Busschots, E. De Clercq, Z. Debyser, and Y. Engelborghs.** 2003. LEDGF/p75 is essential for nuclear and chromosomal targeting of HIV-1 integrase in human cells. J. Biol. Chem. **278**:33528–33539.
51. **Mancebo, H. S., G. Lee, J. Flygare, J. Tomassini, P. Luu, Y. Zhu, J. Peng, C. Blau, D. Hazuda, D. Price, and O. Flores.** 1997. P-TEFb kinase is required for HIV Tat transcriptional activation in vivo and in vitro. Genes Dev. **11**:2633–2644.
52. **Mariani, R., B. A. Rasala, G. Rutter, K. Wiegers, S. M. Brandt, H. G. Krausslich, and N. R. Landau.** 2001. Mouse-human heterokaryons support efficient human immunodeficiency virus type 1 assembly. J. Virol. **75**:3141–3151.
53. **Mariani, R., G. Rutter, M. E. Harris, T. J. Hope, H. G. Krausslich, and N. R. Landau.** 2000. A block to human immunodeficiency virus type 1 assembly in murine cells. J. Virol. **74**:3859–3870.
54. **Masuda, T., V. Planelles, P. Krogstad, and I. S. Chen.** 1995. Genetic analysis of human immunodeficiency virus type 1 integrase and the U3 att site: unusual phenotype of mutants in the zinc finger-like domain. J. Virol. **69**: 6687–6696.
55. **Miller, D. G., and A. D. Miller.** 1994. A family of retroviruses that utilize related phosphate transporters for cell entry. J. Virol. **68**:8270–8276.
56. **Morikawa, Y., S. Hinata, H. Tomoda, T. Goto, M. Nakai, C. Aizawa, H. Tanaka, and S. Omura.** 1996. Complete inhibition of human immunodeficiency virus Gag myristoylation is necessary for inhibition of particle budding. J. Biol. Chem. **271**:2868–2873.
57. **Neil, S., F. Martin, Y. Ikeda, and M. Collins.** 2001. Postentry restriction to human immunodeficiency virus-based vector transduction in human monocytes. J. Virol. **75**:5448–5456.
58. **Newstein, M., E. J. Stanbridge, G. Casey, and P. R. Shank.** 1990. Human chromosome 12 encodes a species-specific factor which increases human immunodeficiency virus type 1 tat-mediated trans activation in rodent cells. J. Virol. **64**:4565–4567.
59. **Nisole, S., and A. Saib.** 2004. Early steps of retrovirus replicative cycle. Retrovirology **1**:9.
60. **Nisole, S., J. P. Stoye, and A. Saib.** 2005. TRIM family proteins: retroviral restriction and antiviral defence. Nat. Rev. Microbiol. **3**:799–808.
61. **Nomura, H., B. W. Nielsen, and K. Matsushima.** 1993. Molecular cloning of cDNAs encoding a LD78 receptor and putative leukocyte chemotactic peptide receptors. Int. Immunol. **5**:1239–1249.
62. **Ory, D. S., B. A. Neugeboren, and R. C. Mulligan.** 1996. A stable human-derived packaging cell line for production of high titer retrovirus/vesicular stomatitis virus G pseudotypes. Proc. Natl. Acad. Sci. USA **93**:11400–11406.
63. **Petit, C., O. Schwartz, and F. Mammano.** 2000. The karyophilic properties of human immunodeficiency virus type 1 integrase are not required for nuclear import of proviral DNA. J. Virol. **74**:7119–7126.
64. **Piller, S. C., L. Caly, and D. A. Jans.** 2003. Nuclear import of the pre-integration complex (PIC): the Achilles heel of HIV? Curr. Drug Targets **4**:409–429.
65. **Planelles, V., A. Haislip, E. S. Withers-Ward, S. A. Stewart, Y. Xie, N. P. Shah, and I. S. Chen.** 1995. A new reporter system for detection of retroviral infection. Gene Ther. **2**:369–376.
66. **Pluymers, W., P. Cherepanov, D. Schols, E. De Clercq, and Z. Debyser.** 1999. Nuclear localization of human immunodeficiency virus type 1 integrase expressed as a fusion protein with green fluorescent protein. Virology **258**:327–332.
67. **Pollard, V. W., and M. H. Malim.** 1998. The HIV-1 Rev protein. Annu. Rev. Microbiol. **52**:491–532.
68. **Popov, S., M. Rexach, G. Zybarth, N. Reiling, M. A. Lee, L. Ratner, C. M. Lane, M. S. Moore, G. Blobel, and M. Bukrinsky.** 1998. Viral protein R regulates nuclear import of the HIV-1 pre-integration complex. EMBO J. **17**:909–917.
69. **Sakai, H., R. Shibata, J. Sakuragi, S. Sakuragi, M. Kawamura, and A. Adachi.** 1993. Cell-dependent requirement of human immunodeficiency virus type 1 Vif protein for maturation of virus particles. J. Virol. **67**:1663–1666.
70. **Sawada, S., K. Gowrishankar, R. Kitamura, M. Suzuki, G. Suzuki, S. Tahara, and A. Koito.** 1998. Disturbed CD4+ T cell homeostasis and in vitro HIV-1 susceptibility in transgenic mice expressing T cell line-tropic HIV-1 receptors. J. Exp. Med. **187**:1439–1449.
71. **Sherman, M. P., and W. C. Greene.** 2002. Slipping through the door: HIV entry into the nucleus. Microbes Infect. **4**:67–73.
72. **Stremlau, M., C. M. Owens, M. J. Perron, M. Kiessling, P. Autissier, and J. Sodroski.** 2004. The cytoplasmic body component TRIM5alpha restricts HIV-1 infection in Old World monkeys. Nature **427**:848–853.
73. **Suzuki, Y., N. Misawa, C. Sato, H. Ebina, T. Masuda, N. Yamamoto, and Y. Koyanagi.** 2003. Quantitative analysis of human immunodeficiency virus type 1 DNA dynamics by real-time PCR: integration efficiency in stimulated and unstimulated peripheral blood mononuclear cells. Virus Genes **27**:177–188.
74. **Tanaka, J., H. Ozaki, J. Yasuda, R. Horai, Y. Tagawa, M. Asano, S. Saijo, M. Imai, K. Sekikawa, M. Kopf, and Y. Iwakura.** 2000. Lipopolysaccharide-induced HIV-1 expression in transgenic mice is mediated by tumor necrosis factor-alpha and interleukin-1, but not by interferon-gamma nor interleukin-6. AIDS **14**:1299–1307.
75. **Tsuruo, T., T. Yamori, K. Naganuma, S. Tsukagoshi, and Y. Sakurai.** 1983. Characterization of metastatic clones derived from a metastatic variant of mouse colon adenocarcinoma 26. Cancer Res. **43**:5437–5442.
76. **Tsurutani, N., M. Kubo, Y. Maeda, T. Ohashi, N. Yamamoto, M. Kannagi, and T. Masuda.** 2000. Identification of critical amino acid residues in human immunodeficiency virus type 1 IN required for efficient proviral DNA formation at steps prior to integration in dividing and nondividing cells. J. Virol. **74**:4795–4806.
77. **van Maanen, M., and R. E. Sutton.** 2003. Rodent models for HIV-1 infection and disease. Curr. HIV Res. **1**:121–130.
78. **Wei, P., M. E. Garber, S. M. Fang, W. H. Fischer, and K. A. Jones.** 1998. A novel CDK9-associated C-type cyclin interacts directly with HIV-1 Tat and mediates its high-affinity, loop-specific binding to TAR RNA. Cell **92**:451–462.
79. **Yang, W. K., J. O. Kiggans, D. M. Yang, C. Y. Ou, R. W. Tennant, A. Brown, and R. H. Bassin.** 1980. Synthesis and circularization of N- and B-tropic retroviral DNA Fv-1 permissive and restrictive mouse cells. Proc. Natl. Acad. Sci. USA **77**:2994–2998.
80. **Yasuda, J., T. Miyao, M. Kamata, Y. Aida, and Y. Iwakura.** 2001. T cell apoptosis causes peripheral T cell depletion in mice transgenic for the HIV-1 vpr gene. Virology **285**:181–192.
81. **Zack, J. A., S. J. Arrigo, S. R. Weitsman, A. S. Go, A. Haislip, and I. S. Chen.** 1990. HIV-1 entry into quiescent primary lymphocytes: molecular analysis reveals a labile, latent viral structure. Cell **61**:213–222.
82. **Zennou, V., C. Petit, D. Guetard, U. Nerhbass, L. Montagnier, and P. Charneau.** 2000. HIV-1 genome nuclear import is mediated by a central DNA flap. Cell **101**:173–185.
83. **Zheng, Y. H., H. F. Yu, and B. M. Peterlin.** 2003. Human p32 protein relieves a post-transcriptional block to HIV replication in murine cells. Nat. Cell Biol. **5**:611–618.

IL-17-Mediated Regulation of Innate and Acquired Immune Response against Pulmonary *Mycobacterium bovis* Bacille Calmette-Guérin Infection[1]

Masayuki Umemura,[2]*‡ Ayano Yahagi,*‡ Satoru Hamada,*§ Mst Dilara Begum,*‡ Hisami Watanabe,† Kazuyoshi Kawakami,¶ Takashi Suda,‖ Katsuko Sudo,# Susumu Nakae,# Yoichiro Iwakura,# and Goro Matsuzaki*‡

IL-17 is a cytokine that induces neutrophil-mediated inflammation, but its role in protective immunity against intracellular bacterial infection remains unclear. In the present study, we demonstrate that IL-17 is an important cytokine not only in the early neutrophil-mediated inflammatory response, but also in T cell-mediated IFN-γ production and granuloma formation in response to pulmonary infection by *Mycobacterium bovis* bacille Calmette-Guérin (BCG). IL-17 expression in the BCG-infected lung was detected from the first day after infection and the expression depended on IL-23. Our observations indicated that γδ T cells are a primary source of IL-17. Lung-infiltrating T cells of IL-17-deficient mice produced less IFN-γ in comparison to those from wild-type mice 4 wk after BCG infection. Impaired granuloma formation was also observed in the infected lungs of IL-17-deficient mice, which is consistent with the decreased delayed-type hypersensitivity response of the infected mice against mycobacterial Ag. These data suggest that IL-17 is an important cytokine in the induction of optimal Th1 response and protective immunity against mycobacterial infection. *The Journal of Immunology,* 2007, 178: 3786–3796.

One-third of the world's population is infected with *Mycobacterium tuberculosis*, with an estimated 8–9 million new cases and 2–3 million deaths from tuberculosis annually (1). Despite the enormous number of people infected, only ~10% of affected individuals show evidence of symptoms and develop the clinical disease. The immunological mechanism for the breakdown of host resistance in these individuals is unclear. Cell-mediated immunity is thought to be the major component of host defense against *M. tuberculosis*. The necessity of $CD4^+$T cells in the control of *M. tuberculosis* in humans is illustrated by the strong association of $CD4^+$T cell impairment and the reactivation of *M. tuberculosis* in patients with HIV infection (2). The reactivation of latent infection that stems from a failure of tissue granulomas to contain the organism (particularly in the lung) has also been reported in experimental models (3).

Although neutrophils are not considered to be effective antimycobacterial effector cells, it has been reported that neutrophils participate in the immune response against mycobacterial infection (4, 5). Depletion of neutrophils at the early stage of mycobacterial infection resulted in an increase of bacterial burden in several reports (5, 6) and reduced pulmonary granuloma formation in another report (7). The depletion of neutrophils roughly 2 wk after mycobacterial infection has been reported to induce an increase in the bacterial count in the lung (8), although the bacterial burden did not increase under similar conditions in another report (5). In contrast, the induction of neutrophils by LPS or rG-CSF resulted in enhanced protection against infection. Because mycobacteria induce cytokine production by neutrophils (5), cytokines are likely candidates in the mechanism of neutrophil-mediated enhancement of protection and granuloma formation. These reports suggest that neutrophils participate in the immune response to mycobacterial infection.

IL-17 is a proinflammatory cytokine secreted by T lymphocytes (9–13) that enhances the generation, activation, and migration of neutrophils through the induction of CXC chemokines, IL-6, IL-8, G-CSF, and TNF (14–16). Studies have shown the importance of IL-17 in various physiological and pathophysiological processes, including the induction of granulopoiesis (17, 18), host defense against *Klebsiella* or *Candida* infections (19, 20), rheumatoid arthritis (21, 22), allograft rejection (23, 24), and asthma (25, 26). IL-17 also triggers neutrophil migration to the lung (15). It has recently been reported that IL-17 is required for the optimal induction of Th1-type and Th2-type immune response, although the mechanism has not yet been clarified (27).

IL-23 was recently identified as a cytokine which induces IL-17 expression (28). IL-23 is a disulfide-bonded heterodimeric cytokine composed of an IL-23-specific p19 subunit and a p40 subunit common to IL-12 and IL-23. It is produced by macrophages and dendritic cells (29). The IL-23R also consists of two components a unique IL-23R subunit (IL-23R) and a subunit shared by IL-12

*Molecular Microbiology Group, and †Immunobiology Group, Center of Molecular Biosciences, University of the Ryukyus, Okinawa, Japan; ‡Division of Host Defense and Vaccinology, Department of Microbiology, and §Division of Child Health and Welfare, Department of Investigative Medicine, Graduate School of Medicine, University of the Ryukyus, Okinawa, Japan; ¶Division of Microbiology and Immunobiology, Department of Medical Technology, School of Health Sciences, Tohoku University and Infection Control Research Center, Tohoku University Hospital, Miyagi, Japan; ‖Division of Immunology and Molecular Biology, Cancer Research Institute, Kanazawa University, Ishikawa, Japan; and #Center for Experimental Medicine, Institute of Medical Science, University of Tokyo, Tokyo, Japan

Received for publication March 24, 2006. Accepted for publication January 5, 2007.

The costs of publication of this article were defrayed in part by the payment of page charges. This article must therefore be hereby marked *advertisement* in accordance with 18 U.S.C. Section 1734 solely to indicate this fact.

[1] This work was supported by grants from the Ministry of Education, Culture, Sports, Science and Technology of Japan, The Naito Foundation, and Takeda Science Foundation.

[2] Address correspondence and reprint requests to Dr. Masayuki Umemura, Molecular Microbiology Group, Center of Molecular Biosciences, University of the Ryukyus, 1 Senbaru, Nishihara, Okinawa 903-0213, Japan. E-mail address: umemura@comb.u-ryukyu.ac.jp

and IL-23 receptors (IL-12Rβ1) (30). The biological functions of IL-12 and IL-23 are similar but not identical. IL-23 is not as potent as IL-12 in the induction of IFN-γ production (29). Instead, IL-23 (but not IL-12) induces the proliferation of memory $CD4^+$ T cells and the IL-17 production of $CD4^+$ T cells (29, 28, 31). IL-23-transgenic mice consistently develop multiorgan inflammation associated with neutrophilia (32). Furthermore, mice deficient in IL-23 but not IL-12 are highly resistant to experimental autoimmune encephalomyelitis, whereas mice deficient in IL-12 but not IL-23 display defective development of Th1-type immune responses (33). A recent study reported that IL-23 enhances protective immunity to *Cryptococcus neoformans* infection and a deficiency of IL-23 is linked to a decrease in IL-17 production (34). All of these results indicate that IL-23 is an important regulator of the inflammatory immune response mediated by IL-17.

The role of IL-23 in mycobacterial infection has also been investigated. Mice lacking both IL-12 and IL-23 (IL-12/23p40-deficient mice) had a higher bacterial burden in *Mycobacterium bovis* bacille Calmette-Guérin (BCG)- or *Mycobacterium tuberculosis*-infected organs than mice deficient in IL-12 alone (IL-12p35-deficient mice) (35, 36). These results suggest an involvement of IL-23 in host defenses against mycobacterial infection. In contrast, an analysis of IL-23p19-deficient mice showed that IL-23 is superfluous in the response to *M. tuberculosis* infection (37). It is therefore controversial whether the IL-23/IL-17 axis is important in protective immunity against mycobacterial infections.

In the present study, we hypothesized that IL-17 participates in the immune response against mycobacterial infection through neutrophil induction and Th1 enhancement. We analyzed IL-17 expression in wild-type mice as well as the immune responses of IL-17 gene-knockout (KO)[3] mice after lung *Mycobacterium bovis* BCG infection. Our results demonstrated that IL-17 is expressed during the early stage of *M. bovis* BCG infection and that IL-23 is required for the induction of IL-17. Although IL-17 is widely considered to be a $CD4^+$ T cell product, we identified TCR $\gamma\delta^+$ T cells and non-T cells as the major IL-17-producing cells during the early stage of infection. Furthermore, the lack of IL-17 resulted in reduced IFN-γ production by mycobacteria-specific $CD4^+$ T cells and impaired granuloma formation after *M. bovis* BCG infection. We will discuss the implications of these results later in this report.

Materials and Methods

Animals

IL-17 gene-KO mice were generated as described previously (27). IL-17 KO mice of (129/Sv × C57BL/6)F_1 hybrid background were backcrossed to the C57BL/6 for more than eight generations. The genotyping of IL-17 KO mice was conducted using the following PCR primers: primer 1, 5′-ACT CTT CAT CCA CCT CAC ACG A-3′; primer 2, 5′-GTA CAC CAG CTA TCC TCC AGA TAG-3′; primer 3, 5′-GCC ATG ATA TAG ACG TTG TGG C-3′. Primers 1 and 2 were used to detect the wild-type allele and primers 1 and 3 were used to detect the mutant allele. IL-12/23p40-deficient mice of C57BL/6 background (38) were purchased from The Jackson Laboratory. TCR Cδ-deficient mice of C57BL/6 background were reported previously (39, 40). C57BL/6 Cr mice were purchased from Japan SLC. All animals were used for experiments at 8–12 wk of age. These mice were kept under conventional conditions in an environmentally controlled clean room at the Center of Molecular Biosciences (University of the Ryukyus, Okinawa, Japan). The experiments were conducted according to the institution's ethical guidelines for animal experiments and the safety guideline for gene manipulation experiments.

[3] Abbreviations used in this paper: KO, knockout; i.t., intratracheally; DTH, delayed-type hypersensitivity; PPD, purified protein derivative; LN, lymph node; PIF, pulmonary infiltrated; BAL, bronchoalveolar lavage fluid; FCM, flow cytometry; Ct, cycle threshold.

Microorganisms and bacterial infection

M. bovis BCG (Japan BCG Association) was grown in 7H9 medium (Difco) supplemented with albumin-dextrose-catalase enrichment (Difco). Small aliquots of *M. bovis* BCG suspended in 7H9 medium containing 10% glycerol were stored at −80°C until use. The viable bacterial numbers were determined by 7H10 (Difco) plate supplemented with oleic acid-albumin-dextrose-catalase enrichment (Difco). The concentration of bacteria was quantified by colony counting. The bacteria were resuspended in PBS before use. Mice were inoculated intratracheally (i.t.) with 5×10^6 CFU of *M. bovis* BCG in 50 μl of PBS. *M. bovis* BCG-infected mice were sacrificed on days 0, 1, 3, 5, 7, 10, 14, 21, and 28. For the in vitro mycobacterial infection of splenocytes, 5×10^6 splenocytes were infected with 5×10^5 CFU of *M. bovis* BCG in 0.5 ml of antibiotic-free RPMI 1640 medium (Sigma-Aldrich) containing 10% heat-inactivated FBS for 90 min and an equal volume of RPMI 1640 containing 10% FBS, 100 U/ml gentamicin was subsequently added. The splenocytes were incubated for either 24 or 48 h.

Delayed-type hypersensitivity (DTH) responses

M. bovis BCG-infected mice were tested for a DTH response to the purified protein derivative (PPD; Japan BCG Association) derived from *M. tuberculosis* by the injection of 10 μg of PPD into the right hind footpad 28 days after the infection. The footpad was measured 24 and 48 h later using a spring-loaded micrometer (Mitutoyo) and the swelling was determined by the following formula: (footpad thickness of the PPD-injected right footpad (millimeter)) − (footpad thickness of the uninjected left footpad (millimeter)).

rIL-17

The stable transfectant producing IL-17 was described previously (41). Briefly, FBL-3 erythroleukemia cells were transfected with pEF-BOS mammalian expression vector (42) carrying the cDNA for full-length mouse IL-17 and pBL-hygB carrying the hygromycin B-resistance gene. Hygromycin B-resistant clones producing the IL-17 were selected. The culture supernatant was collected and the IL-17 concentration was determined and used as rIL-17.

Cell preparation

The lung was perfused with PBS through the right ventricle before excision from the mice. The excised lung tissue, separated from all the associated lymph nodes (LNs), was minced and incubated for 1 h at 37°C in 5 ml of PBS containing 1.0% FBS, 125 U/ml collagenase I (Sigma-Aldrich), 60 U/ml DNase I (Sigma-Aldrich), and 60 U/ml hyaluronidase (Sigma-Aldrich). Single-cell suspensions (pulmonary infiltrated (PIF) cells) were prepared by passing through 30-mm stainless steel mesh. To enrich the pulmonary lymphocytes, PIF cells were resuspended in 8 ml of 45% Percoll solution (Amersham Biosciences), overlaid on 5 ml of 67.5% Percoll solution, and centrifuged at 2200 rpm for 20 min at 20°C. The cells at the interface were collected and used for in vitro culture or flow cytometric analysis. Single-cell suspensions from the mediastinal LNs and spleens were also prepared by passing through 30-mm stainless steel mesh.

Cells in the bronchoalveolar lavage fluid (BAL) were recovered at the indicated times after infection with *M. bovis* BCG. Briefly, the BAL was collected with 1 ml of RPMI 1640 medium containing 10% FBS and 68 mM EDTA. Cells in the BAL were collected and resuspended with 50% FBS-RPMI 1640 medium. Cytospin slides were prepared using a Cytospin model IV (Shandon). Fifty microliters of a 5×10^5 cells/ml cell suspension was placed into the chamber which was attached to cytospin slides, then centrifuged at 800 rpm for 3 min. The cells were morphologically examined after staining with May-Grünwald and Giemsa solutions (Wako Pure Chemical).

Cell culture and ELISA for cytokine production

Single-cell suspensions were prepared in complete RPMI 1640 medium supplemented with 10% FBS. The suspensions (5×10^5 cells in volume of 200 μl of complete RPMI 1640 medium) were added to each well in 96-well plates and incubated in triplicate with or without 5 μg/ml PPD. In some experiments, rIL-17, rIL-23 (R&D Systems), or rIL-12 (PeproTech) was added into the culture. Cells were also cultured in the presence of BCG with or without anti-IL-23p19 Ab (2.5 μg/ml; R&D Systems). The plates were incubated at 37°C in an atmosphere of 5% CO_2 for 24 and 48 h, and the culture supernatants were collected and stored at −30°C until analysis. IFN-γ (R&D Systems), IL-13 (BD Biosciences), IL-23 (eBioscience), and IL-17 (R&D Systems) were assayed by ELISA kits.

Magnetic separation

To enrich T cells, spleen cell suspension was passed through a nylon wool column. The T cell subsets were further fractionated by high-gradient MACS (Miltenyi Biotec). The cells were incubated with FITC-conjugated anti-CD8a (BD Biosciences), PE-conjugated anti-CD4, and allophycocyanin-conjugated anti-CD3e mAbs (BD Biosciences) for 15 min at 4°C. After washing, cells were resuspended and incubated with anti-FITC microbeads (Miltenyi Biotec) for 15 min at 4°C. After another washing step, $CD8^+$ cells were isolated using an AutoMACS (isolation mode: deplete). Negative fractions containing $CD4^+$ and $CD4^-CD8^-$ cells were incubated with anti-PE microbeads (Miltenyi Biotec) for 15 min at 4°C. After washing, $CD4^+$ cells were isolated using an AutoMACS (isolation mode: deplete). Negative fractions containing $CD4^-CD8^-$ cells were incubated with anti-allophycocyanin microbeads (Miltenyi Biotec) for 15 min at 4°C. CD3-positive or -negative $CD4^-CD8^-$ cells were isolated using an AutoMACS (isolation mode: deplete). Aliquots of the unsorted (whole splenocytes) and sorted cell fractions ($CD4^+$, $CD8^+$, $CD3^+CD4^-CD8^-$, and $CD3^-CD4^-CD8^-$ cells) were analyzed by flow cytometry (FCM) as described below. The $CD4^+$, $CD8^+$, $CD3^+CD4^-CD8^-$, and $CD3^-CD4^-CD8^-$ cell populations were sorted to a purity of >98, >98, >95, or >93%, respectively.

Expression of cytokine/chemokine genes

Total RNA was extracted from various organs, such as the lung, mediastinal LNs, or the spleen, using TRIzol reagent (Invitrogen Life Technologies). First-strand cDNA was synthesized from 2 μg of RNA using reverse transcriptase (Superscript II; Invitrogen Life Technologies) and 20 pM of random primer in 20 μl of reaction buffer. The synthesized first-strand cDNA were amplified by quantitative real-time PCR using 20 pM of each primer pair with 2.5 U of the *Taq* polymerase (Takara Shuzo) in a total volume of 20 μl of the reaction buffer consisting of 10 mM Tris-HCl (pH 8.3), 50 mM KCl, 1.5 mM $MgCl_2$, 0.01% gelatin, 0.2 mM dNTP, and SYBR Green I (Cambrex Bio Science). Thermal cycling was initiated with a first denaturation step of 5 min at 95°C, followed by 40 cycles of 95°C for 10 s and 60°C for 30 s. The fluorescence emitted from amplified DNA was read at 60°C at the end of each cycle. The data of the real-time PCR amplification were analyzed using the iCycler iQ and the Real-Time PCR Optical System Software version 3.0 (Bio-Rad). The cycle number at which the various transcripts were detectable, referred to as the threshold cycle (Ct), was compared with that of β-actin and referred to as ΔCt. The relative gene level was expressed as $2^{-(\Delta\Delta Ct)}$, in which ΔΔCt equals ΔCt of the experimental sample minus ΔCt of the control sample. The specific primers were as follows: IL-17 sense (5′-AAG GCA GCA GCG ATC ATC C-3′), IL-17 antisense (5′-GGA ACG GTT GAG GTA GTC TGA G-3′); IL-23p19 sense (5′-CCT GCT TGA CTC TGA CAT CTT C-3′), IL-23p19 antisense (5′-TGG GCA TCT GTT GGG TCT C-3′); IL-12/23p40 sense (5′-ACA TCA AGA GCA GTA GCA GTT C-3′), IL-12/23p40 antisense (5′-AGT TGG GCA GGT GAC ATC C-3′); IL-12p35 sense (5′-CCA CCC TTG CCC TCC TAA AC-3′), IL-12p35 antisense (5′-GGC AGC TCC CTC TTG TTG TG-3′); IL-15 sense (5′-AAA CCC ATG TCA GCA GAT AA-3′), IL-15 antisense (5′-AAG TAG CAC GAG ATG GAT GT-3′); KC sense (5′-TCG CCA ATG AGC TGC GCT GTC-3′), KC antisense (5′-GCT TCA GGG TCA AGG CAA GCC-3′); MIP-2 sense (5′-GAG CTT GAG TGT GAC GCC CCC AGG-3′), MIP-2 antisense (5′-GTT AGC CTT GCC TTT GTT CAG TAT C-3′); G-CSF sense (5′-TCA TTC TCT CCA CTT CCG-3′), G-CSF antisense (5′-GTA TTT ACC CAT CTC CTT CC-3′); IL-6 sense (5′-TCC AGT TGC CTT CTT GGG AC-3′), IL-6 antisense (5′-GTG TAA TTA AGC CTC CGA CTT G-3′); TNF-α sense (5′-TTC TGT CTA CTG AAC TTC GGG GTG ATC GGT CC-3′), TNF-α antisense (5′-GTA TGA GAT AGC AAA TCG GCT GAC GGT GTG GG-3′); β-actin sense (5′-TGG AAT CCT GTG GCA TCC ATG AAA C-3′), and β-actin antisense (5′-TAA AAC GCA GCT CAG TAA CAG TCC G-3′).

In some experiments, expression of IL-17 and β-actin was confirmed by agarose gel electrophoreses of PCR products and staining of the gel with ethidium bromide after adjustment of cDNA amount by the quantitative real-time PCR of β-actin.

Flow cytometric analysis of intracellular cytokine assay

To analyze the IL-17 expression of the cells from the in vitro infection system, spleen cells were incubated with or without *M. bovis* BCG for 48 h at 37°C and 5% CO_2, with GolgiPlug-containing brefeldin A (BD Biosciences) added for the last 8 h in 24-well flat-bottom plates (Nalge Nunc International) in 1 ml of RPMI 1640 medium containing 10% FBS. After 8 h of culture, the cells were harvested and washed once in PBS containing 1.0% newborn calf serum and 0.1% NaN_3 (staining buffer).

To analyze the IL-17 expression of the cells of the in vivo infection system, PIF cells or fractionated pulmonary lymphocytes 3 days after *M. bovis* BCG infection were incubated with or without 1 μg/ml calcium ionophore A-23187 (Calbiochem) and 25 ng/ml PMA (Sigma-Aldrich) for 4 h at 37°C and 5% CO_2 in the presence of GolgiPlug.

The cells were pretreated with culture supernatant from 2.4G2 hybridoma producing mAb specific for FcγR II/III (Fc blocker), and were then surface stained with allophycocyanin-conjugated anti-CD3, NK1.1, CD8α, or CD11b (Mac-1), FITC-conjugated anti-TCR Cβ or Gr-1, and biotin-conjugated anti-TCR Cδ, CD4, or CD45R/B220 (BD Biosciences) mAbs plus TriColor-streptavidin. Surface-stained cells were subjected to intercellular IL-17 staining. For intracellular cytokine staining, we used PE-conjugated anti-IL-17 mAb after permeabilization of the cells using Cytofix/Cytoperm kits (BD Biosciences).

To examine the Ag-specific Th1 immune-response in the in vivo infection system, pulmonary lymphocytes at 7, 14, and 28 days after *M. bovis* BCG infection were incubated with or without 5 μg/ml PPD in the presence of mitomycin C-treated spleen cells (1×10^5 cells) from naive mice for 24 h at 37°C and 5% CO_2, with the addition of GolgiPlug for the last 6 h. Cells were pretreated with Fc blocker, and subsequently surface stained with allophycocyanin-conjugated anti-CD3 mAb. To detect Th1 cells, we used PE-conjugated anti-IFN-γ mAb.

For both intracellular IL-17 and IFN-γ staining, cells were detected by a flow cytometer, FACSCalibur (BD Biosciences). The data were analyzed with CellQuest software (BD Biosciences).

Bacterial counts in organs

Seven, 14, and 28 days after *M. bovis* BCG infection, the mice were sacrificed and their lungs, spleens, and livers were removed. The organs were homogenized in saline containing 0.05% Tween 80. Ten-fold serial dilutions of the homogenates were placed onto Middlebrook 7H10 agar (Difco). The plates were incubated at 37°C for 3 wk. After incubation, the colonies were counted and the bacterial counts in organs were calculated as $\log_{10}$ CFU per organ.

Histopathology

The mice were sacrificed at 3, 7, 14, and 28 days after infection with *M. bovis* BCG. Approximately one-third of the lung and the spleen were fixed in buffered formalin and embedded in paraffin for histopathological examination. Thin sections with 4-mm thickness were prepared and stained with H&E.

To quantify the granuloma area, histological data were acquired using a charge-coupled device camera (Olympus). The digital data were analyzed using the Image J program distributed by the National Institutes of Health. The threshold was set to discriminate between granuloma tissue and normal tissue and the percentage granuloma area was calculated by the Analyze Particle command. Ten to 15 sections were analyzed and the mean and SD of the percentage granuloma area were calculated.

Statistical analysis

The statistical significance of the data was determined by Student's *t* test. A *p* value of <0.05 was considered to indicate a significant difference.

Results

Expression of IL-17 and IL-17-inducing cytokine IL-23 in the lungs of mice inoculated with M. bovis BCG

To assess the involvement of IL-17 in the immune response against mycobacteria, we initially analyzed the expression of IL-17 in the lungs of mycobacteria-infected mice. IL-17 mRNA in the lung of *M. bovis* BCG-infected C57BL/6 mice was detected on day 1 postinfection, peaked on day 5, and then returned to the baseline by day 7 (Fig. 1). We also investigated the factors which induced the IL-17 expression. Other studies have reported that IL-15 and IL-23 are potential inducers of IL-17 production (28, 43). We detected no correlation between IL-15 and IL-17 expression (Fig. 1). In contrast, IL-23p19 expression increased on day 1 and stayed at the same level for up to 3 days (Fig. 1). IL-23p19 expression increased again on day 7 and maintained high expression level up to day 21. IL-12p35 expression also increased on days 1–3, but returned to baseline by day 5. IL-23 is a heterodimeric cytokine consisting of a unique p19 subunit and a p40 subunit shared by IL-12 and IL-23, and IL-12 consists of unique p35 and common

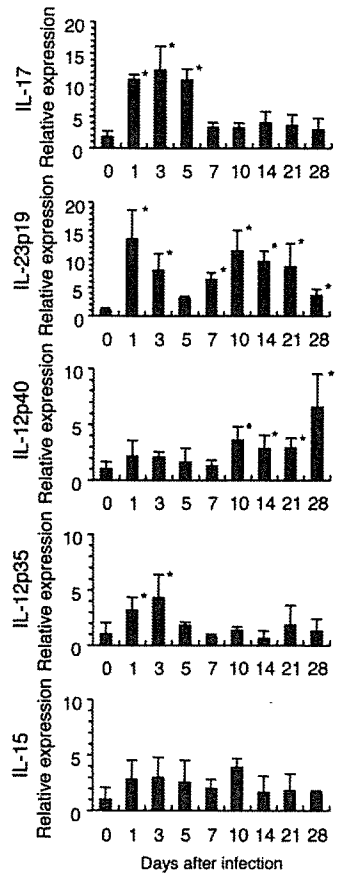

FIGURE 1. Expression of IL-17 and IL-17-inducing cytokines in the lungs of mice i.t. inoculated with *M. bovis* BCG. Wild-type C57BL/6 mice were i.t. inoculated with 5×10^6 CFU of *M. bovis* BCG. Total RNA extracted from the lung was analyzed by quantitative real-time PCR using specific primers. Data are normalized for β-actin RNA content and plotted as fold change over uninfected mice. *, $p < 0.05$ compared with uninfected mice. All the data are representative of three to five separate experiments.

p40. The expression of p40 was not induced at the early stage of infection although its expression was enhanced at a later stage. This finding suggests that constitutively expressed IL-12/23p40 is used to form IL-12 or IL-23. We subsequently tested the involvement of both IL-23 and IL-12 in the induction of IL-17. rIL-23 but not rIL-12 induced IL-17 production in resident pulmonary lymphocytes in a dose-dependent manner, thus suggesting that IL-23 but not IL-12 plays an important role in IL-17 production (Fig. 2*A*). Furthermore, $CD3^+$ T cells in the resident pulmonary lymphocytes were the major IL-17-producing cells significantly induced by rIL-23; however, they were only slightly induced by rIL-12 (Fig. 2*B*). We also found that IL-23 but not IL-12 induced IL-17 production in resident peritoneal exudate cells (44). To further confirm the importance of IL-23 in the induction of IL-17 after *M. bovis* BCG i.t. infection, we infected wild-type and IL-12/23p40 KO mice with *M. bovis* BCG. The expression of IL-17 in the lungs of the IL-12/23p40 KO mice was markedly diminished in comparison to that in the wild-type mice on days 3 and 28 after the *M. bovis* BCG infection (Fig. 2*C*). However, it is still possible that IL-12 contributes to IL-17 induction because IL-12/23p40 KO mice lack both IL-12 and IL-23. To confirm the role of IL-23 in the induction of IL-17 production in the resident pulmonary lymphocytes, the lymphocytes of wild-type mice were infected in vitro with *M. bovis* BCG in the presence or absence of neutralizing Ab to IL-23p19 or control Ig. As shown in Fig. 2*D*, IL-17 expression increased significantly after the mycobacterial infection, while the

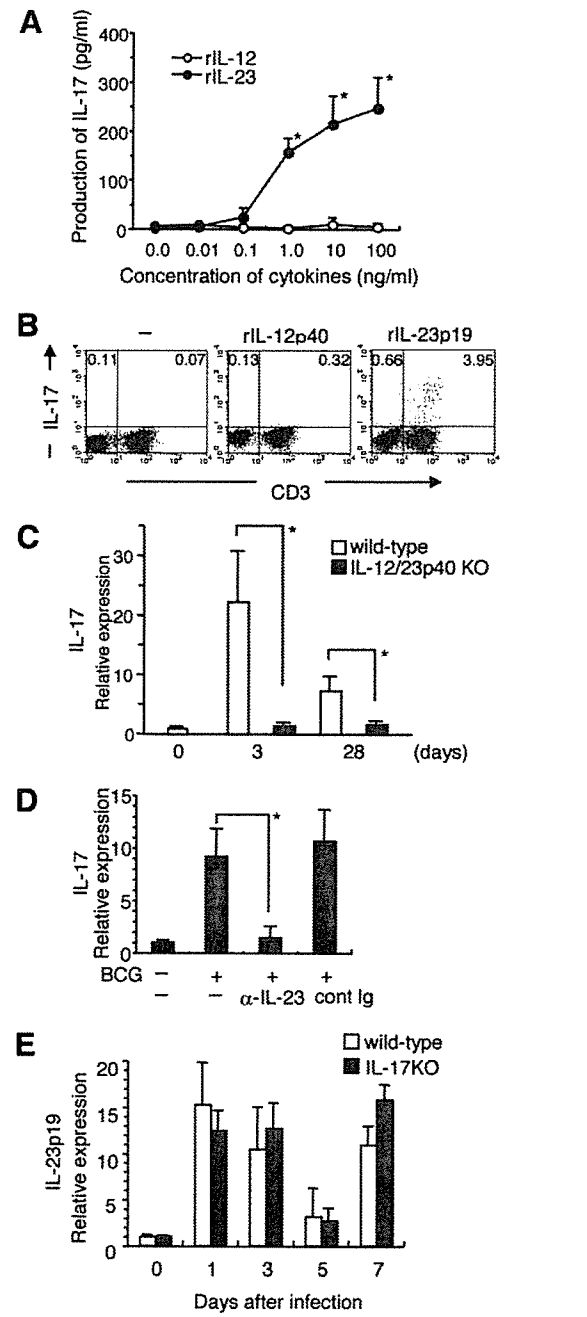

FIGURE 2. IL-23-dependent induction of IL-17 production by the lung cells. *A*, Resident pulmonary lymphocytes were cultured in the presence of different concentrations of rIL-23 or rIL-12. Culture supernatants were collected 24 h later and analyzed for IL-17 production. *, $p < 0.05$ compared with rIL-12-treated cells. *B*, Resident pulmonary lymphocytes were cultured with 10 ng/ml rIL-23 or rIL-12 for 24 h, and with brefeldin A for the last 6 h. After the culture, the cells were surface stained with anti-CD3. Surface-stained cells were subjected to intercellular cytokine staining with anti-IL-17 mAb. Samples were analyzed by FCM. *C*, Wild-type C57BL/6 or IL-12/23p40 KO mice were inoculated i.t. with *M. bovis* BCG. Three and 28 days later, the lungs were collected; total RNA was extracted and analyzed by quantitative real-time PCR using specific primers for IL-17. *, $p < 0.05$ compared with the wild-type mice. *D*, Resident pulmonary lymphocytes of wild-type C57BL/6 mice were infected with *M. bovis* BCG in vitro. Cells were incubated with neutralizing Ab to IL-23p19 or control Ig for 24 h and total RNA was extracted and analyzed by quantitative real-time PCR. *, $p < 0.05$ compared with the culture without Ab. *E*, Wild-type C57BL/6 and IL-17 KO mice were inoculated i.t. with *M. bovis* BCG. The lungs were collected and analyzed by quantitative real-time PCR using primers specific for IL-23p19. All the data are representative of three to five separate experiments.

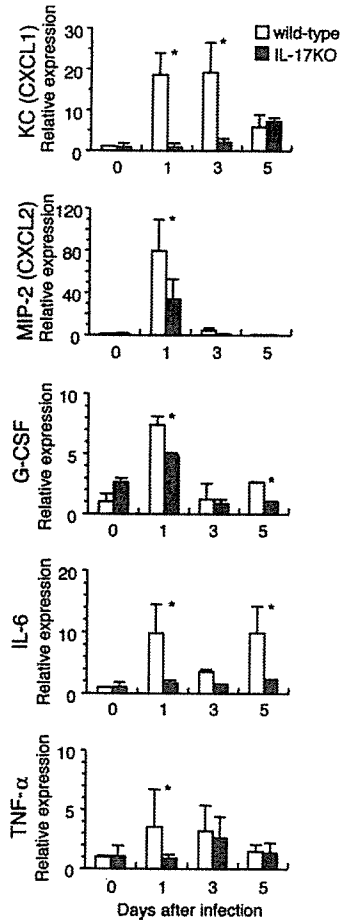

FIGURE 3. Expression of neutrophil-inducing cytokine/chemokine in the lungs of IL-17 KO mice i.t. infected with *M. bovis* BCG. Wild-type C57BL/6 or IL-17 KO mice were inoculated with *M. bovis* BCG. Mice were sacrificed at the indicated times after infection, the lungs were collected, and total RNA was extracted from the lung and analyzed by quantitative real-time PCR using specific primers. *, $p < 0.05$ compared with uninfected mice.

addition of neutralizing Ab to IL-23p19 to the culture suppressed the induction of IL-17 expression. Furthermore, we detected comparable levels of IL-23p19 mRNA (Fig. 2*E*) and IL-23 protein (data not shown) in the lungs of the wild-type and IL-17KO mice after *M. bovis* BCG infection, indicating that IL-23 production is independent of IL-17. These data indicate that IL-23 is required for IL-17 production by *M. bovis* BCG-infected mice.

Impaired neutrophil induction in infected lungs after inoculation with M. bovis *BCG*

It has been reported that IL-17 induces the production of neutrophil CXC chemokines such as human IL-8, murine KC/CXCL1, and murine MIP-2/CXCL2 (45–47). IL-17 also induces the production of cytokines important in the induction, activation, or survival of neutrophils, such as G-CSF, IL-6, and TNF (15, 48). Therefore, we investigated whether IL-17 is responsible for the chemokine/cytokine expression induced by *M. bovis* BCG infection. As shown in Fig. 3, the expression of KC and MIP-2 were severely impaired on days 1–3 and on day 1, respectively, in the lungs of infected IL-17 KO mice in comparison to that in wild-type mice. The expressions of G-CSF, IL-6, and TNF were also diminished in the IL-17 KO mice in comparison to those in the wild-type mice. In findings consistent with the decrease of chemokine/cytokine expression in the IL-17 KO mice, the BAL cells of the IL-17 KO mice contained significantly lower number of neutrophils on days 1–5 after infection (Table I). These results indicate that IL-17 participates in the induction of acute neutrophil-mediated inflammation in the lungs of *M. bovis* BCG-infected mice. In addition, the numbers of monocytes and lymphocytes in the BAL cells of the IL-17 KO mice were also lower in comparison to the wild-type mice after *M. bovis* BCG infection (Table I).

Identification of IL-17-expressing cells in response to M. bovis *BCG infection in vitro*

We established an in vitro infection system to determine the phenotype of IL-17-producing cells at the early stage of mycobacterial infection. Splenocytes from naive wild-type mice were infected with *M. bovis* BCG in vitro and were separated into several fractions after 24 and 48 h of culturing. The expression of IL-17 was subsequently analyzed by RT-PCR. Unexpectedly, strong IL-17 mRNA expression was detected in the $CD4^-CD8^-$ cells (Fig. 4*A*). Because spleen TCR $\gamma\delta^+$ T cells are $CD4^-CD8^-CD3^+$ T cells, we theorized that $CD4^-CD8^-CD3^+$TCR $\gamma\delta^+$ T cells produce IL-17 in the culture system. Therefore, $CD4^-CD8^-$ cells were separated into CD3-positive or -negative populations and analyzed. The expression of IL-17 induced by *M. bovis* BCG infection was detected not only in $CD4^-CD8^-CD3^+$ T cells but also in $CD4^-CD8^-CD3^-$ (non-T) cells (Fig. 4*B*, *left panels*), thus indicating that IL-17 is expressed by both TCR $\gamma\delta^+$ T cells and non-T cells. To confirm the expression of IL-17 by TCR $\gamma\delta^+$ T cells, an in vitro infection analysis was conducted using spleen cells from TCR Cδ KO mice. IL-17 expression of $CD4^-CD8^-CD3^+$ T cells was markedly reduced in the TCR Cδ KO mice (Fig. 4*B*, *right panels*). Interestingly, IL-17 production by $CD4^-CD8^-CD3^-$

Table I. *Subsets of the BAL from wild-type mice or IL-17KO mice after BCG infection*[a]

	Days	Total Cells	Neutrophils	Monocytes	Lymphocytes ($\times 10^7$ cells)
Wild type	0	4.51 ± 0.37	0.003 ± 0.009	4.27 ± 0.18	0.12 ± 0.12
	1	15.50 ± 4.99	10.10 ± 2.11	3.38 ± 1.27	1.51 ± 1.38
	3	50.04 ± 14.39	23.32 ± 5.80	19.48 ± 5.89	5.88 ± 1.86
	5	33.46 ± 8.80	3.23 ± 2.24	15.29 ± 2.94	12.86 ± 2.61
IL-17KO	0	4.53 ± 0.38	nd	4.29 ± 0.18	0.18 ± 0.12
	1	3.93 ± 0.56**	0.26 ± 0.16**	3.35 ± 0.25	0.25 ± 0.08*
	3	25.97 ± 5.84**	12.64 ± 2.05**	10.89 ± 2.55**	1.94 ± 0.89**
	5	9.66 ± 2.92*	0.97 ± 0.38*	3.38 ± 1.08**	5.07 ± 1.33**

[a] The BAL fluid was recovered at the indicated times after infection with *M. bovis* BCG. Cells were morphologically examined after staining with May-Grünwald and Giemsa solutions and then counted by microscopy. The values from the IL-17KO mice were significantly different from the values for wild-type mice infected with *M. bovis* BCG (*, $p < 0.005$; **, $p < 0.001$; nd, not detectable).

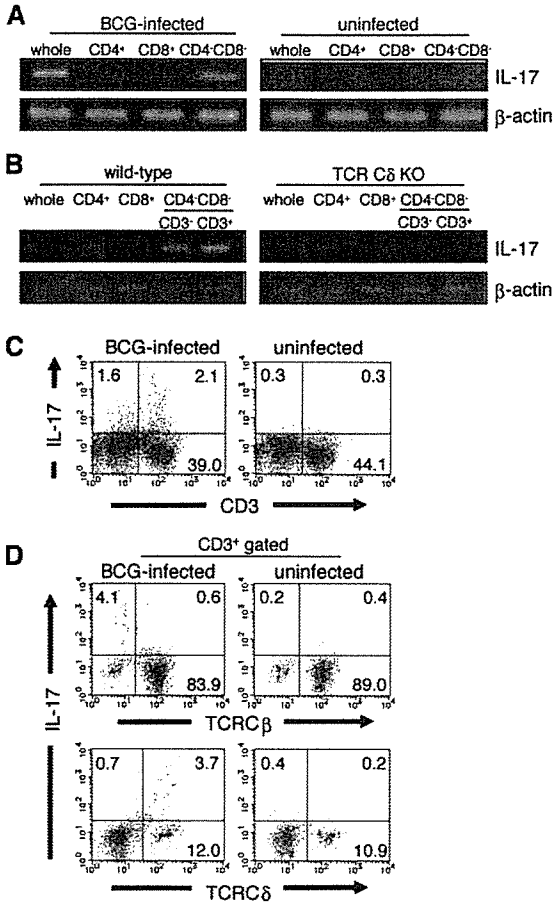

FIGURE 4. Identification of $CD4^-CD8^-$ TCR $\gamma\delta^+$ T cells as the major IL-17-expressing cells in response to *M. bovis* BCG infection in vitro. *A* and *B*, Spleen cells of wild-type C57BL/6 (*A*) or TCR Cδ KO mice (*A* and *B*) were infected with *M. bovis* BCG in vitro. Cells were collected and separated by magnetic cell sorting after 48 h of the culture and the expression of IL-17 was analyzed by RT-PCR. *C* and *D*, Spleen cells of C57BL/6 mice were infected with *M. bovis* BCG in vitro. After 40 h of culture, GolgiPlug was added and the cells were incubated for another 8 h. The cells were then surface-stained with allophycocyanin-anti-CD3, FITC-anti-TCR Cβ, and biotin-anti-TCR Cδ mAbs plus TriColor-streptavidin. Surface-stained cells were subjected to intercellular cytokine staining with PE-anti-IL-17 mAb. Samples were analyzed by FCM. The IL-17 expression of total spleen cells (*C*) or $CD3^+$ cells (*D*) is shown. Data representative of three independent experiments are demonstrated in all panels.

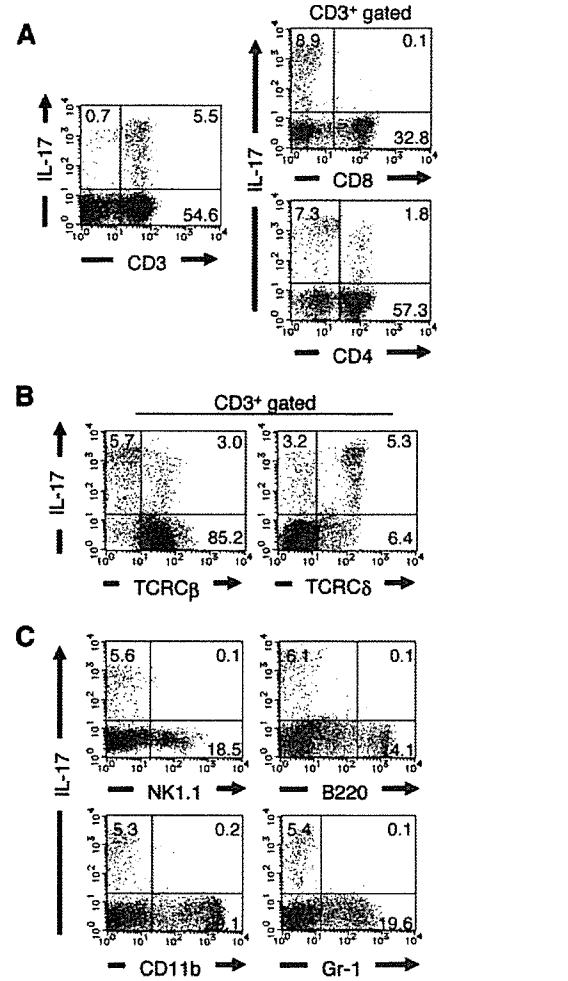

FIGURE 5. Identification of TCR $\gamma\delta^+$ T cells as IL-17-producing cells after *M. bovis* BCG infection of the lung in vivo. Wild-type C57BL/6 mice were infected i.t. with *M. bovis* BCG. The PIF cells were collected 3 days after infection and cultured with or without 1 μg/ml calcium ionophore A-23187 and 25 ng/ml PMA for 4 h at 37°C and 5% CO_2 in the presence of GolgiPlug. The cells were surface-stained with allophycocyanin-conjugated anti-CD3, NK1.1, CD8α, or CD11b (Mac-1), FITC-conjugated anti-TCR Cβ or Gr-1, and biotin-conjugated anti-TCR Cδ, CD4, or CD45R/B220 mAbs plus TriColor-streptavidin. Surface-stained cells were subjected to intercellular cytokine staining. For intracellular cytokine staining, we used PE-conjugated anti-IL-17 mAb after the permeabilization of the cells. The IL-17 expression in lung lymphocytes in the PIF cells (*A–C*, *upper panels*) or whole PIF cells (*C*, *lower panels*) are shown. Lymphocytes in the PIF cells were gated on $CD3^+$ cells (*A*, *right panels*; *B*). Data representative of three independent experiments are demonstrated in all the panels.

(non-T) cells was also decreased in the TCR Cδ KO mice after infection.

To confirm IL-17 is expressed by $CD4^-CD8^-$ cells at the protein level, in vitro *M. bovis* BCG-infected or uninfected splenocytes were stained for cell surface markers and cytoplasmic IL-17 and analyzed by FCM. Consistent with the RT-PCR results shown in Fig. 4*B*, both the $CD3^+$ T cells and $CD3^-$ non-T cells from *M. bovis* BCG-infected splenocytes produced IL-17 (Fig. 4*C*). Among the $CD3^+$ cells, the TCR $C\delta^+$ and TCR $C\beta^+$ cells produced IL-17, although $C\delta^+$ T cells represented >80% of the IL-17-producing T cells (Fig. 4*D*). The ratio of IL-17-producing cells in TCR $C\delta^+$ cells (~45%) was higher than that in TCR $C\beta^+$ cells (~3%).

To confirm IL-17 production by TCR $\gamma\delta^+$ T cells and non-T cells in vivo in the mycobacteria-infected lung, we i.t. infected the wild-type mice with *M. bovis* BCG, and analyzed the IL-17 expression by PIF cells and pulmonary lymphocytes. $CD3^+$ T cells were the major IL-17-producing cells in the infected lungs, although $CD3^-$ non-T cells produced IL-17 as well (Fig. 5*A*, *left panel*). To determine which T cells produce IL-17 upon *M. bovis* BCG-infection, pulmonary lymphocytes were stained with mAb against CD4 or CD8 and IL-17, and analyzed by FCM. Approximately 20% of the IL-17^+ $CD3^+$ T cells were $CD4^+$, but the remaining IL-17-producing T cells were the $CD4^-CD8^-$ phenotype (Fig. 5*A*, *right panels*). Among the $CD3^+$ T cells, both the TCR $C\beta^+$ and TCR $C\delta^+$ T cells produced IL-17 (Fig. 5*B*). The ratio of IL-17-producing cells in TCR $C\delta^+$ T cells (~45%) was higher than that in TCR $C\beta^+$ T cells (~3.5%). In addition, the mean fluorescence intensity of IL-17 staining of the TCR $C\delta^+$ T cells (2150.6) was higher than that of the TCR $C\beta^+$ T cells (425.1). These results indicate that TCR $\gamma\delta^+$ T cells produce IL-17 at a higher frequency and intensity than TCR $\alpha\beta^+$ T cells. The data indicate that TCR $\gamma\delta^+$ T cells are the major

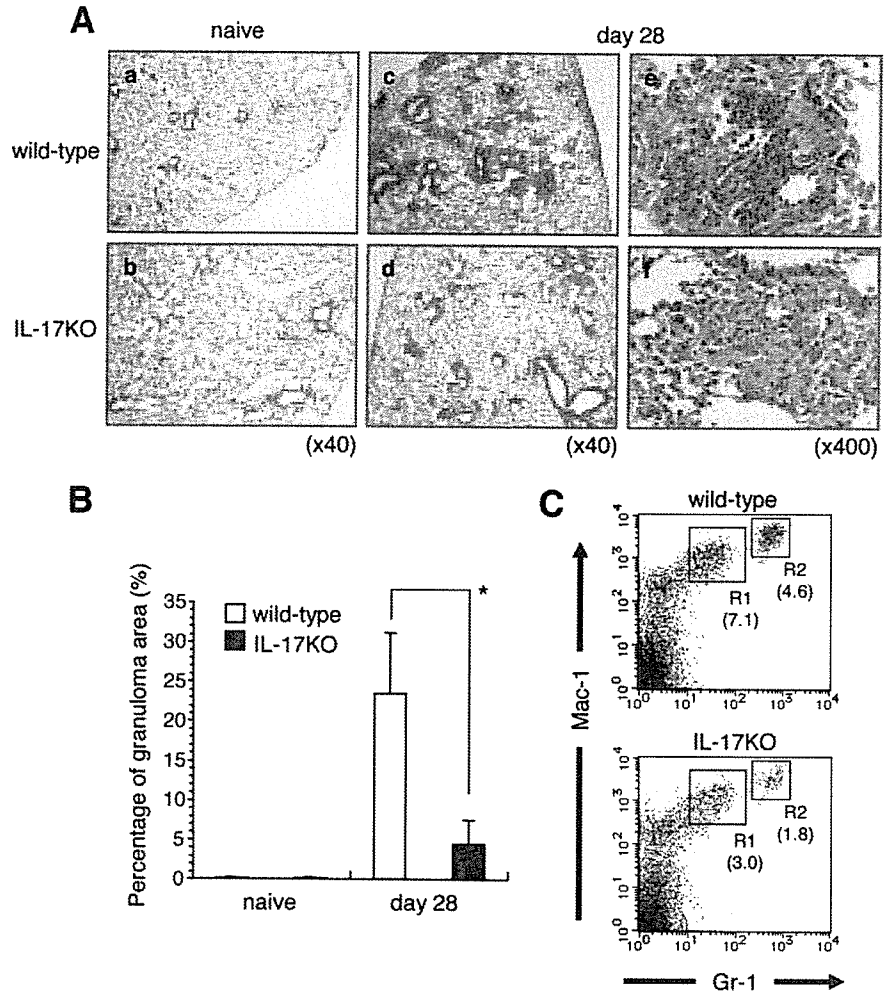

FIGURE 6. Reduction of granuloma size in the lung and DTH reaction to PPD of IL-17 KO mice after *M. bovis* BCG lung infection. Wild-type C57BL/6 or IL-17 KO mice were inoculated i.t. with *M. bovis* BCG. *A*, Mice were sacrificed 4 wk after infection and formalin-fixed sections were stained with H&E. Lung tissues from naive C57BL/6 mice (*a*), naive IL-17 KO mice (*b*), BCG-infected C57BL/6 mice (*c* and *e*), and BCG-infected IL-17 KO mice (*d* and *f*) are shown. Original magnification, ×40 (*c* and *d*) and ×400 (*e* and *f*). Data representative of three separate experiments are shown. *B*, The percentage granuloma area of 10–15 sections was analyzed, and the mean and SD of percentage granuloma area is shown. *C*, Mice were sacrificed 4 wk after i.t. infection. The cells were prepared from the lung and stained with Mac-1 and Gr-1 mAbs for FCM. R1 represents lung macrophages, whereas R2 represents neutrophils. Representative results from four separate experiments are shown in each panel.

IL-17-producing cells in vivo. We further investigated the markers of IL-17-producing non-T cells. However, we could not detect IL-17 production in NK1.1$^+$, CD45R/B220$^+$, CD11b$^+$, or Gr-1$^+$ cells (Fig. 5*C*).

Impaired granuloma formation in the lungs of IL-17 KO mice infected with M. bovis *BCG*

Because the participation of neutrophils in granuloma formation was suggested, and IL-17 itself was reported to enhance the Th1 response, we hypothesized that a lack of IL-17 during mycobacterial infection influences the establishment of the acquired immune response and granuloma formation. A histological examination was conducted on the lungs of *M. bovis* BCG-infected IL-17 KO mice on day 28 of infection, when the acquired immune response and granulomas were established in the lungs of the wild-type mice (Fig. 6). The size and number of granulomas in the lungs of the IL-17 KO mice were reduced in comparison to the granulomas in the wild-type mice on day 28 of infection (Fig. 6, *A* and *B*). The granulomas in the lungs of the IL-17 KO mice were less densely packed with mononuclear cells in comparison to those in the wild-type mice (Fig. 6*A*, *e* and *f*). This result indicates that IL-17 is an important factor in the establishment of granulomas.

To further compare the cellular composition in the granulomas of the wild-type and the IL-17 KO mice, FCM analysis of monocyte and granulocyte lineage markers was conducted on PIF cells on day 28 after i.t. *M. bovis* BCG infection. As shown in Fig. 6*C*, the ratios of CD11b$^+$Gr-1^{low} macrophages (R1 of the Fig. 6*C*) and CD11b$^+$Gr-1^{high} neutrophils (R2) were lower in the lungs of the IL-17KO mice than those in the wild-type mice. In contrast, the ratio of macrophages to granulocytes in the infected lungs of IL-17 KO mice (~1:0.6) was nearly identical with that in the wild-type mice. These results suggest that the accumulation of both monocytes and granulocytes was reduced in the granulomas in the IL-17 KO mice.

Impaired IFN-γ production by mycobacterial Ag-specific T cells and DTH in the IL-17 KO mice after infection with M. bovis *BCG*

We investigated whether the absence of IL-17 affected the Ag-specific Th1 immune response to mycobacterial Ags after i.t. infection with *M. bovis* BCG. On day 14 after infection, there was no statistically significant difference in IFN-γ production by pulmonary lymphocytes in the wild-type and IL-17 KO mice, although IL-17KO mice tended to show slightly lower levels of production (Fig. 7*A*). On day 28 after infection, the lung lymphocytes from the IL-17 KO mice showed a significantly lower level of IFN-γ production than those from the wild-type mice ($p < 0.01$). In contrast, IL-4 and IL-13 were not produced in the pulmonary lymphocytes of either the wild-type or the IL-17 KO mice at any stage of *M. bovis* BCG infection (data not shown), indicating that the diminished IFN-γ production in the IL-17KO mice was not due to a deviation to the Th2-type immune response. To determine the population of IFN-γ-producing cells, we analyzed the CD3$^+$ pulmonary lymphocytes by intracellular IFN-γ staining and FCM analysis (Fig. 7*B*). T cells from the IL-17 KO mice showed a slightly

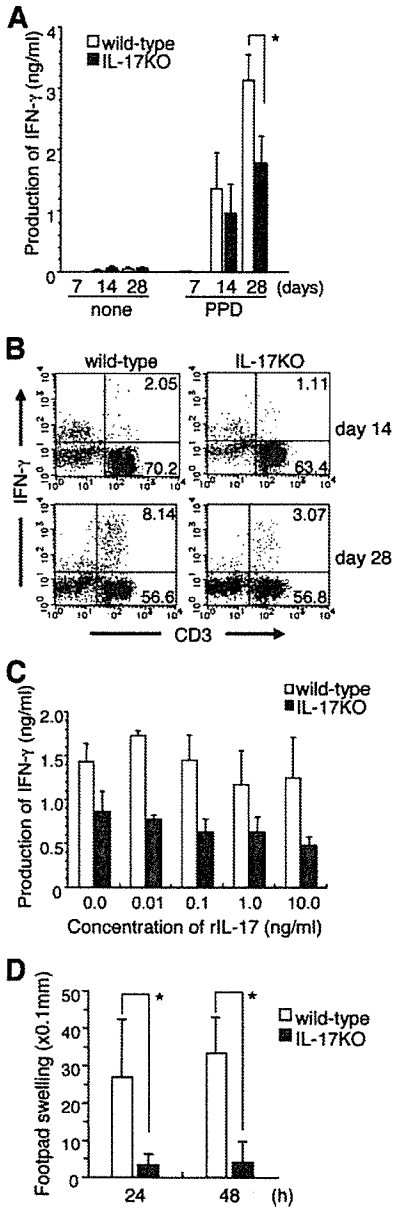

FIGURE 7. Impairment of IFN-γ production by Ag-stimulated lymphocytes and DTH in IL-17 KO mice after infection with *M. bovis* BCG. *A*, Mice were inoculated i.t. with *M. bovis* BCG. The PIF cells (5×10^5 cells) were cultured on day 7, 14, or 28 after infection with PPD (5 μg/ml) in the presence of naive spleen APC (1×10^5 cells) for 24 h at 37°C. The concentrations of IFN-γ in the culture supernatants were determined by ELISA. Statistical analysis was performed with Student's *t* test. *, Significant difference ($p < 0.01$). *B*, Lymphocytes of the lung were collected from the mice of each group after infection and cultured with 5 μg/ml PPD for 18 h at 37°C and with GolgiPlug for the last 6 h. After the culture, the cells were surface stained with allophycocyanin-conjugated anti-CD3. Surface-stained cells were subjected to intercellular cytokine staining with PE-conjugated anti-IFN-γ mAb. Samples were analyzed by FCM. *C*, The lymphocytes in the lung (2×10^5 cells) on day 28 after infection were cultured with the indicated concentrations of rIL-17 and PPD (5 μg/ml) in the presence of spleen APC (2×10^4 cells) for 24 h at 37°C. After the incubation period, the concentrations of IFN-γ in the culture supernatants were determined by ELISA. *D*, Four weeks after infection, the mice were injected s.c. with 10 μg of PPD into the right hind footpads. Specific footpad swelling was measured 24 and 48 h later and data are expressed as the mean ± SD. *, $p < 0.05$ compared with the wild-type mice. Representative results from three separate experiments are shown in each panel.

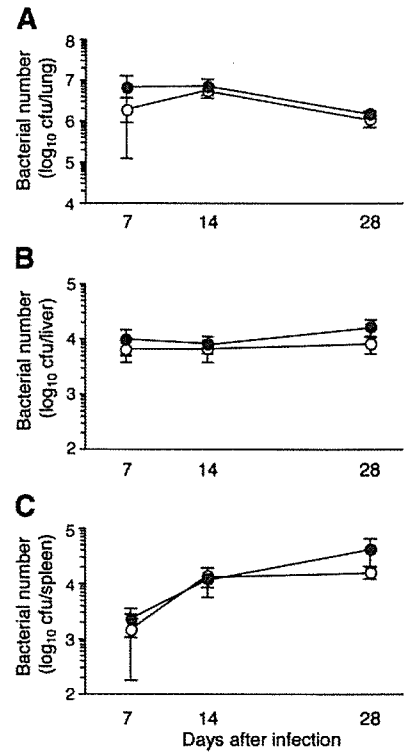

FIGURE 8. Bacterial growth in infected organs of IL-17 KO mice after *M. bovis* BCG infection. Mice were inoculated i.t. with *M. bovis* BCG and CFU in the lungs (*A*), livers (*B*), and spleens (*C*) were determined on days 7, 14, and 28 after infection. Open symbols and closed symbols, The wild-type mice and the IL-17 KO mice, respectively.

lower percentage of IL-17-producing cells (1.7% of $CD3^+$ T cells) in comparison to that of the wild-type mice (2.8% of $CD3^+$ T cells) (Fig. 7*B*, *upper panels*). The ratio of IFN-γ-producing cells was significantly lower in the T cells from the IL-17 KO mice than that from the wild-type mice (5.1 ± 0.7% in the IL-17 KO mice vs 11.7 ± 1.4% in the wild-type mice) on day 28 after infection ($p < 0.01$). These results indicated that the generation of Th1 cells was impaired in IL-17 KO mice infected with *M. bovis* BCG at 4 wk.

It is possible that IL-17 directly induced IFN-γ production of T cells. To examine the possibilities, we stimulated the pulmonary lymphocytes on day 28 after infection with graded concentrations of rIL-17. rIL-17 did not affect the IFN-γ production of the pulmonary lymphocytes from either the wild-type or the IL-17 KO mice (Fig. 7*C*). These results suggest that IL-17 is not a direct inducer of IFN-γ production in T cells.

To further investigate the cell-mediated immune response in the IL-17 KO mice, we evaluated the ability of the IL-17 KO mice to mount DTH responses. We sensitized the wild-type and IL-17 KO mice by *M. bovis* BCG infection, elicited DTH responses 4 wk later by injection of PPD into the right hind footpads, and measured specific footpad swelling 24 and 48 h after the challenge. We found that the DTH to mycobacterial Ag was inhibited in the IL-17 KO mice in comparison to that of wild-type mice (Fig. 7*D*). Therefore, IL-17 is indispensable to the optimal induction of DTH responses and a lack of IL-17 leads to an inefficient cell-mediated immune response.

Bacterial loads of various organs in IL-17 KO mice after infection with M. bovis *BCG*

To analyze the role of IL-17 in protective immunity against mycobacterial infection, we examined the bacterial growth in various

organs of the wild-type and IL-17 KO mice after i.t. infection with *M. bovis* BCG. As shown in Fig. 8, the bacterial numbers in the lungs, livers, and spleens of the IL-17 KO mice were similar to those in the wild-type mice on days 7, 14, and 28 after infection. The data suggest that IL-17 is superfluous during the early protective immune response that suppresses bacterial expansion in the infected organs.

Discussion

In this study, we demonstrate that IL-17 plays a key role in neutrophil induction after pulmonary mycobacterial infection. The recruitment of neutrophils to the lungs has been described in patients in the acute phase of tuberculosis (49, 50) and in experimental animals infected with mycobacteria (51, 52), but the molecular mechanism was not clarified. To determine the involvement of IL-17 in the induction of neutrophils in response to mycobacterial infection, we analyzed the migration of neutrophils to the lungs in the *Mycobacterium*-infected IL-17KO mice. We demonstrated that neutrophil mobilization in the *M. bovis* BCG-infected lungs was significantly suppressed in the IL-17-deficient mice. Furthermore, IL-17 was induced in the lung from an early stage of *M. bovis* BCG pulmonary infection in the wild-type mice. These results demonstrate the importance of IL-17 in the induction of neutrophils after *M. bovis* BCG infection. The macrophage/DC-derived cytokines IL-23 and IL-15 have been reported to induce IL-17 production (28, 43). We identified IL-23 as an IL-17 inducer in pulmonary mycobacterial infection because IL-17 production was significantly suppressed in the IL-12/23p40-deficient mice and IL-12 failed to induce IL-17 (Ref. 53 and this report). Because the expression of neutrophil-inducing chemokines KC/CXCL1 and MIP-2/CXCL2 and neutrophil-inducing/activating cytokines G-CSF and IL-6 was also decreased in the absence of IL-17, IL-17-mediated neutrophil induction may depend on these chemokines and cytokines. IL-17 has been reported to be an important mediator of neutrophil migration and host defense against pneumonia by *Klebsiella pneumoniae* (19, 53). In the experimental model of *Klebsiella* infection, it was suggested that bacterial products induce a subset of T cells to secrete IL-17. A similar mechanism may be involved in mycobacteria-induced neutrophil migration.

In this study, we found that TCR $\gamma\delta^+$ T cells and unidentified non-T cells were the major IL-17-producing cells in the mycobacteria-infected spleen and lung. It has been reported that IL-17 is produced by TCR$\alpha\beta^+$CD4$^-$CD8$^-$ thymocytes (54) as well as by activated CD4$^+$ and CD4$^+$CD45RO$^+$ memory T cells (9). Activated CD8$^+$ and CD8$^+$CD45RO$^+$ memory T cells are also produce IL-17 in humans (55). However, we previously reported that both TCR $\alpha\beta^+$ T cells and TCR $\gamma\delta^+$ T cells produced IL-17 after stimulation with the Fas ligand (41). The ratio of IL-17-producing cells in the TCR $\gamma\delta^+$ T cells was higher than that in the TCR $\alpha\beta^+$ T cells. Among the T cell subset identified by CD4/CD8 expression, CD4$^-$CD8$^-$ cells were the major producers of Fas ligand-induced IL-17, although some CD4$^+$CD8$^-$ cells produced it as well. This distribution of IL-17-producing T cell subsets in *M. bovis* BCG-infected spleen cells is similar to that observed in Fas ligand-induced IL-17 production. We confirmed that both TCR $\alpha\beta^+$ T cells and TCR $\gamma\delta^+$ T cells produce IL-17 in splenocytes and pulmonary lymphocytes after *M. bovis* BCG infection (Figs. 4*D* and 5*B*). The percentage of IL-17-producing TCR $\gamma\delta^+$ T cells among the IL-17-producing T cells (~60–70%) was higher than that of IL-17-producing TCR $\alpha\beta^+$ T cells. It is noteworthy that the proportion of IL-17-producing cells among the TCR $\gamma\delta^+$ T cells (~45%) was higher than that in the TCR $\alpha\beta^+$ T cells (~3.5%) after *M. bovis* BCG infection, and that the mean fluorescence intensity of IL-17 staining is higher in TCR $\gamma\delta^+$ T cells than TCR $\alpha\beta^+$ T cells. These observations suggest that TCR $\gamma\delta^+$ T cells are the major IL-17-producing cells in our system. Furthermore, a portion of IL-17-producing cells were non-T cells without CD3 expression (Figs. 4*C* and 5*A*). Recently, it was reported that neutrophils produce IL-17 in a model of LPS-induced lung inflammation (56); however, no IL-17 production by neutrophils was detected in our system. The identification of IL-17-producing non-T cells is ongoing.

The role of neutrophils at the early stage of mycobacterial infection is controversial. Several in vitro studies suggested that human neutrophils are able to kill virulent *M. tuberculosis* (57, 58) but other reports failed to reproduce the result (59). A recent report demonstrated the increased bacterial burden in infected organs from the early stage of mycobacterial infection when neutrophils are depleted from mice before and/or during this stage (6). However, another report failed to detect any difference in the bacterial counts in the neutrophil-depleted mice (60). We demonstrated that the absence of IL-17 resulted in a significant reduction of neutrophil accumulation in the lung (Table I and Fig. 6*C*) without compromising the control of bacterial growth on days 7–28 after infection (Fig. 8). The data indicate that IL-17-induced neutrophils themselves are not effective effector cells in the elimination of mycobacteria at the early stage of infection before the establishment of acquired immunity. Although neutrophils may not act as direct effector cells against mycobacteria, they may serve as important immunoregulators. Cytokines and chemokines are produced by mycobacteria-activated neutrophils (7, 61). Furthermore, Ab-mediated neutrophil depletion resulted in the formation of disorganized granulomas in the mycobacteria-infected lung (7). This observation is similar to that seen in the IL-17 KO mice. We hypothesize that the IL-17-induced migration of neutrophils into the lung may have an important role in the formation of organized granulomas.

Our data further demonstrate that IL-17 is an important cytokine not only in the early neutrophil recruitment but also in the induction of Th1-type acquired immunity after pulmonary mycobacterial infection. The IL-17 KO mice showed a decreased level of mycobacterial Ag-specific Th1 response on day 28 after *M. bovis* BCG infection. It has been reported that IL-17 is required to induce optimum Th1 and DTH responses against haptens (27), which is consistent with our observation that the Th1-type response is decreased in the absence of IL-17. However, IL-17 failed to directly enhance mycobacterial Ag-specific IFN-γ production because the level of IFN-γ production was not altered when the T cells from the *M. bovis* BCG-infected IL-17 KO mice were cultured with rIL-17 (Fig. 7*C*). This finding is consistent with a report showing that exogenously added IL-17 affected neither Th1/Th2 phenotype differentiation nor IL-17 production (62). Yao et al. (63) reported that IL-17 stimulates the activity of the transcriptional factor NF-κB, which is known to up-regulate gene products involved in cell activation and growth control. Therefore, we speculate that IL-17-mediated NF-κB activation of APCs or other immunoregulatory cells may be important in the induction of an optimum level of Th1 response. The mechanism of IL-17-mediated enhancement of the Th1 response is now under investigation.

In summary, we investigated IL-17 production and IL-17-mediated immune regulation in mycobacterial infection. We found that IL-23-induced IL-17 production in *M. bovis* BCG-infected mice in vivo and infected spleen cells in vitro. The major IL-17 producers were TCR $\gamma\delta^+$ T cells. IL-17 induced by *M. bovis* BCG infection affected not only early pulmonary neutrophil induction,